Noise and respiration component reduction for non-contact heart rate measurement based on Doppler radar

ドップラーレーダを基にする非接触心拍検出のための雑音及び呼吸成分除去

January, 2024

Moushumi Tazen

Acknowledgments

This paper is a summary of the research conducted in the Information and Communication Laboratory, Department of Information and Electronics Engineering, Faculty of Engineering, Tottori University.

I would like to express our sincere gratitude to Professor Naoto Sasaoka, Professor Tadao Nakagawa, and Professor Isao Nakanishi for their warm guidance and advice in conducting this research.

I would like to express our deep gratitude to all the faculty members of the Department of Electrical and Electronic Engineering, Faculty of Engineering, Tottori University for their various support in carrying out this research.

I would like to thank Mr. Takumi Honjo, Mr. Hashimoto Ryohei, Mr. Shunsuke Fukuya, and Mr. Moaekawa of the Department of Electrical and Electronic Engineering, Faculty of Engineering, Tottori University, who have continued their research together, for their valuable discussions.

In addition, Mr. Kosuke Yoshinaga, Mr. Hajime Kobayashi of the Information and Communication Laboratory, Department of Electrical and Electronic Engineering, Tottori University, who cooperated in the preparation of this paper from beginning to end.

January, 2024

<Table of Contents>

LIST OF ABBREVIATION AND TECHNICAL SYMBOLS

Symbols	Symbols Definitions
f_c	Carrier frequency
t	Time Index
ϕ	Phase noise
d_0	Distance
x	Motion of the subject's chest
t_d	Time delay
R	Received signal
θ_0	Phase change
λ	Wavelength
h	Heart rate
r	Respiration
m	Amplitude
f	Frequency
$\hat{f}$	Notch frequency
I/Q	Complex signal
ρ	Pole radius
β	Tap coefficient
S	Sampling
n	Number of samples
μ	Step size
$*$	Complex conjugate
M	Number of stages

NLMS	Normalized least mean square
e	Filter
RHEF	Respiration harmonic elimination filter
c	Cumulant
τ	Time delay
E[]	Expected value
MAPE	Mean absolute percentage error
MAE	Mean absolute error
MSE	Mean squared error
RMSE	Root mean squared error

Chapter 1
Introduction

In recent years, with the advent of an aging society, interest in monitoring biological information has increased. Currently, problems include an increase in the number of elderly people living alone and an increase in lifestyle-related diseases. Along with this, interest in the daily monitoring of biological information for daily health management is increasing. Monitoring biological information such as heartbeat and breathing rate is effective for early detection of illness or sudden changes in physical condition and is also an important indicator in the medical field. Many conventional biomonitoring systems require electrodes to be brought into contact with the user's body for measurement, which poses the problem of placing a large burden on the user due to discomfort and a sense of restraint caused by the contact.

Furthermore, animals have come to live together with humans as important members of their owners' families. As a result, there is a growing demand for high-level medical care similar to that of humans, but even if animals sense something unusual about their bodies, it is difficult for them to tell their owners. For this reason, monitoring of heart rate, respiratory rate, etc. has been adopted as an effective means to detect diseases and changes in physical condition and is also considered an important indicator in the medical field. However, since many animals refuse to be touched by electrodes, it may be uncomfortable to measure heart rate and respiratory rate using an electrocardiogram monitor, which is a typical example of a contact sensor.

Therefore, a heartbeat/respiration rate detection system using Doppler radar is attracting attention as a non-contact sensing method for biological information. This system obtains heart rate and respiratory rate by observing the minute movements of the heart and breathing that appear on the body surface. Compared to conventional contact-type biological information sensing, it is non-contact and non-restrictive and can be measured even when wearing clothes, making it much more convenient. Examples of applications that have been proposed include monitoring systems for elderly people while they are sleeping, monitoring

the condition of drivers while driving a vehicle, and detecting human bodies hidden in rubble during disasters.

Therefore, there is a need to sense biological information without contact, and heart rate/respiration rate detection systems using Doppler radar are attracting attention. There are always periodic and minute vibrations associated with breathing and heartbeat on the body's surface. Monitoring can be performed by detecting these minute vibrations with Doppler radar and calculating respiration and heartbeat through signal processing.

In non-contact heart rate and breathing rate detection using Doppler radar, detection accuracy deteriorates significantly due to body movement noise and respiratory harmonics that interfere with the heartbeat. The research was conducted with the aim of improving the accuracy of heart rate estimation by removing interference caused by respiratory harmonics and factors that degrade estimation accuracy. In the experiment, measurements are performed using a Doppler radar with a carrier frequency of 24 GHz, and the optimal parameters for computer simulation are investigated. I also confirm the effectiveness of our method by comparing the conventional method and the proposed method.

The research conducted based on the technical background consists of two chapters:

Chapter 2: A novel heart rate estimation method is proposed that uses an adaptive notch filter (ANF). The proposed system estimates respiration frequency. Next, cascaded notch filters, the notch frequencies of which are controlled by the estimated respiration frequency, eliminate respiration harmonics; thus, the accuracy of heart rate estimation improves [1]-[27].

Chapter 3: This chapter investigates the suitability of bispectrum estimation for extinguishing the influence of the received signal. The bispectrum represents the dependency between two different frequency spectra. Assuming that the heart-beat component from the subject has a strong phase coupling, the bispectrum estimation of a received signal enhances the heart-beat component. Then the influence and noise can be reduced. The experimental results showed the bispectrum estimation improved the estimation accuracy of heart rate [28]-[37].

Chapter 2
Non-contact Heart Rate Measurement Based on Adaptive Notch Filter and Elimination of Respiration Harmonics

2. Introduction

Non-contact heart rate estimation is effective because it allows long-term monitoring without needing to attach uncomfortable sensors to the body. Therefore, heartbeat and respiration rate detection systems using a Doppler radar have been attracting attention as they can collect biometric information in a non-contact manner. In recent years, animals are increasingly being treated as family members, and the expectations for their health care and management are correspondingly high. However, animals cannot communicate their health needs to humans; moreover, attaching contact sensors, such as an electrocardiogram (ECG), to exhausted animals causes discomfort and adds an additional burden on veterinarians. Consequently, the use of non-contact sensors on animals has attracted increased research interest. Periodic and minute vibrations associated with breathing and heartbeat are prevalent on the body's surface. These minute vibrations can be detected using a Doppler radar and monitored by estimating respiration and heartbeat rates [1]. Juan et al. attempted to measure the respiration rate of a rat using a Doppler radar [2].

In addition to Doppler radar, Garbey et al. used thermal imaging for non-contact measurements in humans [3]. This method is based on the property that superficial vessels radiate thermal signals and their temperature changes with blood flow. Parnandi et al. proposed using an eye tracker to measure heart rate from pupillary fluctuations [4]. This method takes advantage of the fact that pupillary and heart rate fluctuations are under the control of the autonomic nervous system. Photoplethysmography (PPG)-based methods were also proposed to utilize the human face information obtained through a camera [5]-[8]. They can detect the heartbeat from the green channel fluctuations because it features most

characteristics of plethysmographic signals corresponding to hemoglobin absorption. A method using HSV, a color space different from RGB, has also been proposed [9]. Another technique uses face images obtained from visible and infrared videos [10]. Unfortunately, conventional methods [3]-[10] use videos of human faces or pupils, rendering them difficult to apply on animals because animals' skin is not visible because their bodies, including their faces, are covered with hair, and pupil detection requires restraint of the animal. Therefore, in this study, I focused on the Doppler radar-based method.

Many systems have been proposed for heart rate measurement using a continuous-wave Doppler radar, which is simple and low-cost. Droitcour developed a heart rate estimation system that involves a peak search of the autocorrelation or amplitude spectrum based on a fast Fourier transform (FFT) [1]. This system requires a long time window to maintain a high-frequency resolution. Li et al. introduced the RELAX algorithm for parametric and cyclic optimization to estimate heartbeat and respiration frequency [11]. Tariq et al. developed a system that uses a continuous wavelet transform (CWT), which has a higher time-frequency resolution than FFT [12].

A received Doppler radar signal contains respiration and heartbeat components, as well as moving artifacts and noise. Respiration harmonics in the frequency band of the heartbeat component degrade the accuracy of heart rate estimation. Moving artifacts are generated by the body's movement. An animal moves around in a cage during heart-rate measurements. The bodies of animals also slightly and rapidly tremble regardless of respiration or heartbeat, generating moving artifacts. Therefore, Tu et al. proposed a method to reduce respiration harmonics [13]. However, the method is not practical because it uses an extremely long time window to estimate the frequency and power of respiratory harmonics. Subsequently, Tu et al. proposed a practical system that uses multiple FFTs with different window lengths to eliminate respiration harmonics [14]. However, moving artifacts still degraded estimation performance. In addition, Mogi et al. proposed a method based on spectrograms [15]. This method takes advantage of positive and negative frequencies corresponding to cardiac motion and is robust against respiration harmonics, small moving artifacts, and noise.

Petrovi et al. and Son et al. proposed heart rate estimation methods using moving averages and bandpass filters (BPF) for extracting the heartbeat component [16], [17]. Petrovi et al. use a narrow bandpass filter bank (BPFB) [16]. This method switches a bandpass filter to the other bandpass filter of the band containing the heartbeat component and then eliminates respiration harmonics that are out of the band of the selected bandpass filter. In [17], the data recovery procedure doubles the estimated heart rate if the estimated heart rate is excessively low. Yang et al. proposed adaptive noise cancellation and a new-type discrete cosine transform (N-DCT) to remove artifacts caused by random body motion [18]. However, this method assumes that the velocity of body motion is constant within a short time window, but in general, the velocity of random body motion is not constant; therefore, this assumption may degrade the estimation performance. Chen et al. proposed the heart-rate measurement based on difference quadratic sum demodulation to prevent the generation of respiration harmonics [19]. This method requires estimating the heart rate from the components with frequencies corresponding to doubled heart rate, doubled respiration rate, and the sum of respiration and heart rate. However, the unexpected components, other than the three abovementioned frequencies, occur because of the body movement, and the estimation accuracy is degraded.

In this chapter, a heart rate estimation method is proposed that is robust against respiration harmonics, moving artifacts, and noise. The proposed method uses an infinite impulse response-based adaptive notch filter (IIR-ANF) [20], [21] for estimating the respiration frequency in a low-frequency band that is occupied by the respiration component. Subsequently, cascaded notch filters, with notch frequencies corresponding to respiration harmonics, prevent interference with heartbeat components. These cascaded notch filters are composed of all-pass filters with substantially narrow notch bands and minimize heartbeat component loss. Finally, the proposed method estimates heart rate using an ANF with an adaptive algorithm from the output signal of cascaded notch filters. An ANF based on an all-pass filter with an adaptive algorithm can accurately estimate a notch frequency without the influence of white noise [22]. Animals have large respiration harmonics due to their large body movement, and humans have low respiration harmonics due to low body movement.

The proposed method improves the accuracy of heart rate estimation in the presence of moving artifacts and noise.

This chapter is organized as follows: In Section II, a Doppler radar and the frequency spectrum of a received signal are discussed. The proposed heart rate estimation system, which is robust against respiration harmonics, moving artifacts, and noise, is detailed in Section III. The measurement experiment conducted to evaluate the proposed system is discussed in Section IV. Finally, the paper is concluded in Section V.

2.1 Doppler Radar

A non-contact heart rate estimation system detects minute periodic vibrations on the body surface caused by a heartbeat from a reflected microwave. Assuming that amplitude is ignored, the transmit signal of a Doppler radar is expressed as [1],

$$T(t) = \cos[2\pi f_c t + \phi(t)], \tag{2.1}$$

where f_c is the carrier frequency, t is the time index, and $\phi(t)$ is the phase noise of an oscillator. Assuming that the reference distance between a Doppler radar and the subject is d_0 and that the displacement due to the motion of the subject's chest is $x(t)$, the distance to the chest from the Doppler radar is expressed as $d(t) = d_0 + x(t)$. When, the chest fluctuates before the microwave reaches the subject, the distance between the Doppler radar and the chest is $d(t - (d(t)/c))$ at the moment the signal reflects. Therefore, the time delay t_d between transmission and reception can be expressed as [1]

$$t_d = \frac{2d\left(t - \frac{d(t)}{c}\right)}{c} = \frac{2\left\{d_0 + x\left(t - \frac{d(t)}{c}\right)\right\}}{c}, \tag{2.2}$$

The respiration-induced chest movement is a 5-cm sinusoid with a 5-second period [1]. However, when d_0 is 1 m, d_0/c is 0.33×10^{-8} seconds. As the motion cycle of the chest is sufficiently larger than d_0/c, the term $d(t)/c$ can be ignored. The received signal of the Doppler radar is delayed by t_d as expressed in (2.2). When $x(t) \ll d_0$, the received signal

$R(t)$ can be approximated as the following equation using (2.1) and (2.2) [1].

$$R(t) \approx \cos\left[2\pi f_c t - \frac{4\pi d_0}{\lambda} - \frac{4\pi x\left(t - \frac{d(t)}{c}\right)}{\lambda} + \phi\left(t - \frac{2d_0}{c} - \frac{2x\left(t - \frac{d(t)}{c}\right)}{c}\right) + \theta_0\right], \quad (2.3)$$

where θ_0 is the phase change on the reflecting surface, and $\lambda = c/f_c$ is the wavelength.

Next, the received signal is multiplied by the transmission signal to only extract the phase shift due to chest movement. The Doppler radar can obtain baseband in-phase/quadrature (I/Q) signals as expressed by the following equations [1].

$$I(t) = \cos\left\{\theta' + \frac{4\pi x(t)}{\lambda} + \Delta\phi(t)\right\} + DC_I, \quad (2.4)$$

$$Q(t) = \sin\left\{\theta' + \frac{4\pi x(t)}{\lambda} + \Delta\phi(t)\right\} + DC_Q,$$

where $\theta^I = 4\pi d_0/\lambda - \theta_0$ and $\Delta\varphi(t) = \varphi(t) - \varphi(t - 2d_0/c)$. DC_I and DC_Q are DC offset components in I/Q signals, respectively. Subsequently, the Doppler radar system analyzes the orthogonal I and Q signals.

Then, the effect of respiration components on heart rate estimation is explored using the Fourier series expansion of I/Q signals. The displacement due to chest movement $x(t)$ is expressed as [23]

$$\begin{aligned} x(t) &= x_r(t) + x_h(t) \\ &\approx m_r sin(2\pi f_r t + \psi_{r0}) + m_h sin(2\pi f_h t + \psi_{h0}), \end{aligned} \quad (2.5)$$

where, $x_r(t)$ and $x_h(t)$ represent the physiological movement generated by respiration and heartbeat, respectively. These can be generally modeled as sinusoids with respective: amplitudes as m_r and m_h; frequencies as $f_r$and f_h; and initial phases ψ_{r0} and ψ_{h0}, Using (2.5), I/Q signals are represented by the following equations [23].

$$I(t) = cos\left[\frac{4\pi x_r(t)}{\lambda} + \frac{4\pi x_h(t)}{\lambda} + \Phi\right] + DC_I$$

$$= DC_I + \sum_{k=-\infty}^{\infty}\sum_{l=-\infty}^{\infty} J_k\left(\frac{4\pi m_r}{\lambda}\right) J_l\left(\frac{4\pi m_h}{\lambda}\right).cos(2\pi k f_r t + 2\pi l f_h t + \Phi), \quad (2.6)$$

$$Q(t) = sin\left[\frac{4\pi x_r(t)}{\lambda} + \frac{4\pi x_h(t)}{\lambda} + \Phi\right] + DC_Q$$

$$= DC_Q + \sum_{k=-\infty}^{\infty}\sum_{l=-\infty}^{\infty} J_k\left(\frac{4\pi m_r}{\lambda}\right) J_l\left(\frac{4\pi m_h}{\lambda}\right).sin(2\pi k f_r t + 2\pi l f_h t + \Phi), \quad (2.7)$$

where the phase term is represented as $\Phi = \theta' + \Delta\phi(t)$ for simplicity. $J_p(\cdot)$ represents the Bessel function of the first kind of *p-th* order. Equations (2.6) and (2.7) indicate that *I/Q* signals comprise the fundamental wave of respiration and its harmonics; the fundamental wave of heartbeat and its harmonics; and the intermodulation wave of respiration and heartbeat. Consequently, respiration harmonics degrades heart rate estimation accuracy.

2.2 Heart Rate Estimation System

2.2.1 Structure of Adaptive Notch Filter System

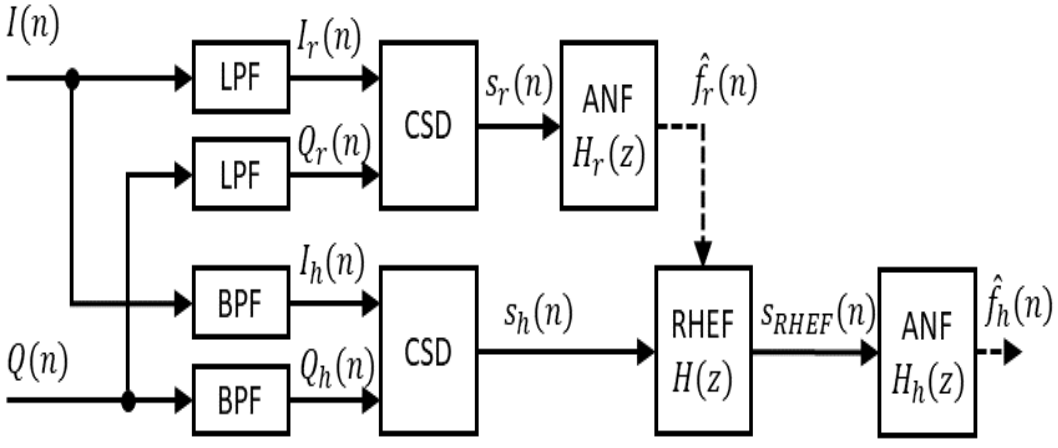

FIGURE 2.1. Structure of the proposed system.

The proposed heart rate estimation system uses an ANF to eliminate respiration harmonics. Fig. 2.1 shows the flow of the proposed system, comprising a bandpass filter (BPF), low pass filter (LPF), complex signal demodulation (CSD) component, ANF $H_r(z)$ for estimating respiration frequency, respiration harmonics eliminating filter (RHEF) $H(z)$, and another ANF $H_h(z)$ for estimating heartbeat frequency.

I/Q signals from (2.4), are converted into discrete-time signals of $I(n)$ and $Q(n)$, where n represents the time index for a discrete-time signal. First, *I/Q* signals are filtered by the LPF and BPF to separate respiration and heartbeat components. Because respiration frequency is generally smaller than heartbeat frequency, the LPF obtains the fundamental wave of respiration. The BPF separates the components, including heartbeat and respiration harmonics, from the fundamental wave of respiration. The output *I/Q* signals of the LPF are represented as $I_r(n)$ and $Q_r(n)$ respectively. Similarly, the output *I/Q* signals of the BPF are represented as $I_h(n)$ and $Q_h(n)$, respectively.

Next, the CSD component is used for combining I/Q signals [23]. The cosine and sine of Φ in (2.6) and (2.7) respectively, determine the relative strength between even-order and odd-order harmonics. Therefore, the heart rate is difficult to detect because of phase Φ. To solve this problem, the CSD component reconstructs complex signals from I/Q signals. The respective complex input signals for $H_r(z)$ and $H_h(z)$ are represented as [23].

$$S_r(n) = I_r(n) + j.Q_r(n) \quad (2.8)$$
$$S_h(n) = I_h(n) + j.Q_h(n) \quad (2.9)$$

$H_r(z)$ estimates the respiration frequency as a notch frequency $\widehat{f_r}(n)$ of $H_r(z)$ from $S_r(n)$. This filter is explained in detail in Section III-B. Next, $H(z)$ which comprises cascaded notch filters, eliminates respiration harmonics from $S_h(n)$. The output signal of $H(z)$ is represented as $s_{RHEF}(n)$. Section III-C explains the RHEF $H(z)$ in detail. Finally, $H_h(z)$ estimates the heartbeat frequency as a notch frequency $\widehat{f_h}(n)$ of $H_h(z)$. The structure of this filter is described in Section III-D. The estimated heart rate $HR_{est}(n)$ (beats per minute (bpm)) is obtained by multiplying $\widehat{f_h}(n)$ by 60.

2.2.2 Respiration Frequency Estimation

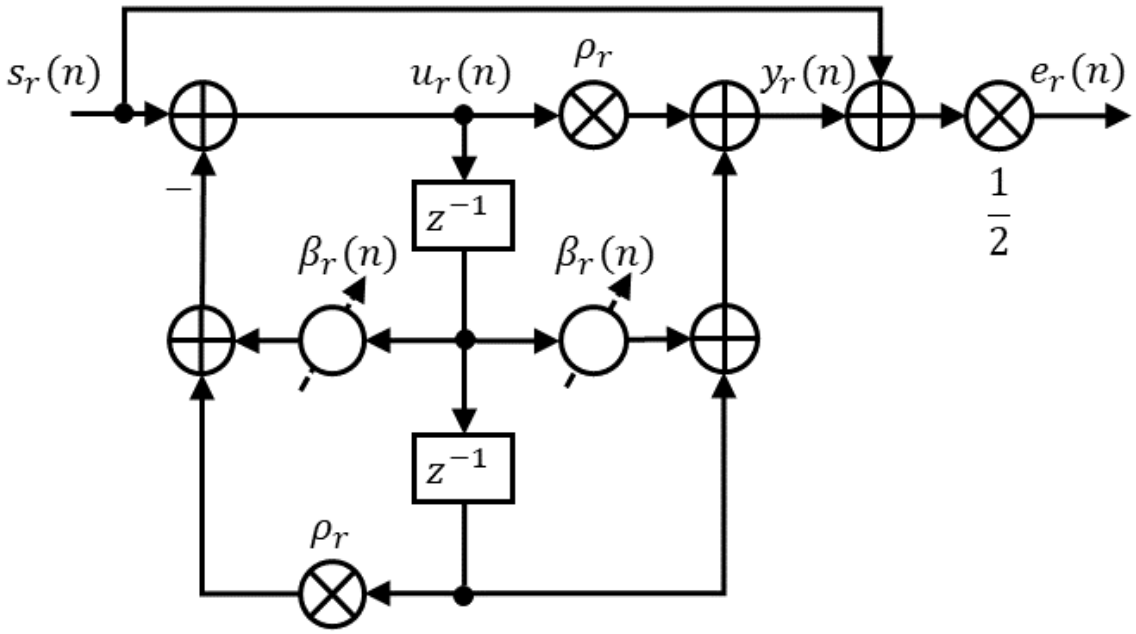

FIGURE 2.2. Structure of ANF for estimating respiration frequency.

Respiration frequency $f_r(n)$ is estimated using $H_r(z)$. The ANF $H_r(z)$ comprises a 2nd order IIR filter, which has all-pass filter characteristics. The structure of this filter is illustrated in Fig. 2.2. The transfer function $H_r(z)$ is given by [24]

$$H_r(z) = \frac{1}{2} \cdot \frac{1 + \rho_r + 2\beta_r z^{-1} + (1 + \rho_r) z^{-2}}{1 + \beta_r z^{-1} + \rho_r z^{-2}}, \tag{2.10}$$

where ρ_r is the squared pole radius of $H_r(z)$, and $\beta_r(n)$ is the tap coefficient related to an estimated respiration frequency $\hat{f}_r(n)$. The output $e_r(n)$ of $H_r(z)$ is represented as

$$e_r(n) = \frac{1}{2}\{s_r(n) + y_r(n)\}, \tag{2.11}$$

where $y_r(n)$ is an output signal of the 2nd order IIR filter in $H_r(z)$ and expressed as

$$y_r(n) = \rho_r u_r(n) + \beta_r u_r(n-1) + u_r(n-2), \tag{2.12}$$

where $u_r(n)$ is a tap input signal of the 2nd order IIR filter.

$\beta_r(n)$ controls the notch frequency at which the magnitude response $H_r(z)$ becomes zero as follows [24].

$$\beta_r(n) = -(1+\rho_r)cos2\pi\left(\frac{f_r(n)}{F_s}\right), \tag{2.13}$$

where F_s is the sampling frequency. Since $s_r(n)$ is occupied by the fundamental wave of respiration, the respiration frequency is estimated as the notch frequency. Using (2.13), the estimated respiration frequency $\widehat{f_r}(n)$ is given by

$$\widehat{f_r}(n) = \frac{F_s}{2\pi}cos^{-1}\left\{\frac{\beta_r(n)}{1+\rho_r}\right\}, \tag{2.14}$$

The tap coefficient $\beta_r(n)$ is updated using the following complex normalized least mean square (NLMS) algorithm [25].

$$\beta_r(n+1) = \beta_r(n) - \mu_r\frac{e_r(n)u_r^*(n-1)}{u_r^2(n-1)}, \tag{2.15}$$

where μ_r represents the step size. $*$ denotes the complex conjugate.

2.2.3 Respiration Harmonic Elimination

RHEF $H(z)$ consists of cascaded notch filters. Moreover, notch frequencies are determined by the estimated respiration frequency $\widehat{f_r}(n)$, and its transfer function is given by

$$H(z) = \prod_{m=1}^{M}\frac{1}{2}\cdot\frac{(1+\rho)+2\beta_m(n)z^{-1}+(1+\rho)z^{-2}}{1+\beta_m(n)z^{-1}+\rho z^{-2}}, \tag{2.16}$$

where M represents the number of stages of a notch filter, ρ represents the squared pole radius, and β_m represents the tap coefficient corresponding to the $(m+1)-th$ harmonic frequency of respiration. $\beta_m(n)$ is expressed as [24]

$$\beta_m(n) = -(1+\rho)\cos\{2\pi\frac{(m+1)\hat{f}_r(n)}{F_s}\}, \tag{2.17}$$

The notch frequencies of $H(z)$ change according to the estimated respiration frequency $\hat{f}_r(n)$. Thus, the proposed system can obtain a signal that attenuates the respiration harmonics interfering with heartbeat components as the output signal of $H(z)$. The notch band of notch filters is substantially narrow, and the RHEF minimizes the loss of heartbeat components.

2.2.4 Heart Rate Frequency Estimation

The transfer function $H_h(z)$ is expressed as [24]

$$H_h(z) = \frac{1}{2}\cdot\frac{1+\rho_h+2\beta_h(n)z^{-1}+\left(1+\rho_h\right)z^{-2}}{1+\beta_h(n)z^{-1}+\rho_h z^{-2}}, \tag{2.18}$$

where ρ_h is the squared pole radius of $H_h(z)$, and $\beta_h(n)$ is the tap coefficient related to heart rate. The output of this filter $e_h(n)$ is represented as

$$e_h(n) = \frac{1}{2}\{s_{RHEF}(n) + y_h(n)\}, \tag{2.19}$$

where $y_h(n)$ is an output signal of the 2nd order IIR filter in $H_h(z)$ and expressed by

$$y_h(n) = \rho_h u_h(n) + \beta_h u_h(n-1) + u_h(n-2), \tag{2.20}$$

where $u_h(n)$ is a tap input signal of the 2nd order IIR filter in $H_h(z)$.

The estimated heartbeat frequency $\hat{f}_h(n)$ is defined from the notch frequency and tap coefficient $\beta_h(n)$, as follows:

$$\hat{f}_h(n) = \frac{F_s}{2\pi}cos^{-1}\left\{\frac{\beta_h(n)}{1+\rho_h}\right\}, \tag{2.21}$$

using the relationship between a notch frequency of an ANF and tap coefficient [24]. The tap coefficient $\beta_h(n)$, is updated using the following complex NLMS algorithm [25].

$$\beta_h(n+1) = \beta_h(n) - \mu_h \frac{e_h(n)u_h^*(n-1)}{u_h^2(n-1)}, \tag{2.22}$$

where μ_h represents the step size for $H_h(z)$.

Let us consider the influence of moving artifacts and noise on an ANF with NLMS algorithm. The numerator of the updating term $e_h(n)u_h^*(n-1)$ represents instantaneous estimates of $E[e_h(n)u_h^*(n-1)]$ in a steepest-descent algorithm. Moreover, the least mean square algorithm, which is recursive, effectively estimates $E[e_h(n)u_h^*(n-1)]$ using time averaging [25]. When the input signal of the ANF is white, $E[e_h(n)u_h^*(n-1)]$ is zero because of the orthogonality associated with an all-pass filter [22]. Thus, assuming that noise and moving artifacts are white in nature, they do not influence heart rate estimation. Even if noise and moving artifacts are colored (no-white) in nature, an ANF with the NLMS algorithm is expected to eliminate their influence in the case that their frequency characteristics are close to white. Moreover, in case where an animal suddenly moves, e.g., sitting and then standing posture, moving artifacts occur suddenly and their probability characteristics drastically change in a short time duration. As the adaptive algorithm neglects the moving artifact components in $E[e_h(n)u_h^*(n-1)]$ due to the time-variance of a moving artifact, an ANF with the NLMS algorithm is robust against moving artifacts.

2.3 Measurement Experiment

2.3.1 Doppler Radar Setup and Evaluation

A computer simulation is conducted to evaluate the performance of the proposed system. The Doppler radar module used in this experiment is the SHARP DC6M4JN3000 with one transmitter antenna and one receiver antenna. Its carrier frequency is 24 GHz with a maximum output power of 10 dBm. The H plane and E plane beam widths are 25° and 20° respectively. The gain of the horn antennas is 20 dBi. The module comprises the LPF and BPF. It outputs discrete-time I/Q signals ($I_r(n)$, $Q_r(n)$, $I_h(n)$, and $Q_h(n)$, with a 50-Hz sampling frequency.

To evaluate the estimated heart rate, used the mean absolute percentage error (MAPE), mean absolute error (MAE), mean squared error (MSE), and root mean squared error (RMSE) which were defined as

$$MAPE = \frac{1}{K}\sum_{i=1}^{K}\frac{\left|HR_{ref}(i) - HR_{est}(i)\right|}{HR_{ref}(i)} \times 100[\%], \tag{2.23}$$

$$MAE = \frac{1}{K}\sum_{i=1}^{K}\left|HR_{ref}(i) - HR_{est}(i)\right|, \tag{2.24}$$

$$MSE = \frac{1}{K}\sum_{i=1}^{K}\left\{HR_{ref}(i) - HR_{est}(i)\right\}^2, \tag{2.25}$$

$$RMSE = \sqrt{\frac{1}{K}\sum_{i=1}^{K}\left\{HR_{ref}(i) - HR_{est}(i)\right\}^2}, \tag{2.26}$$

where $|\cdot|$ represents the absolute value, K is the number of samples, $HR_{est}(i)$ is the estimated heart rate at the $i-th$ sample, and $HR_{ref}(i)$ is the heart rate measured by a contact-type device.

2.4 Measurement Experiments for Human Subjects

2.4.1 Measurement Conditions for human subjects

This section provides details of the experiments conducted on humans who can remain stationary to evaluate only the reduction performance of the respiration harmonics of the proposed method. Table 2.1 lists the parameters of the proposed system used in this experiment. The NLMS algorithm converges if and only if $0 < \mu < 2$ [25]. When μ is 1, the convergence speed of the NLMS algorithm is fastest [26]. If tap input signals include disturbance and optimal tap coefficients are nonstationary, the optimum step size is given by the signal to noise ratio (SNR) of the tap input signal and the power of optimal tap coefficient fluctuation [27]. As the SNR and power of the optimal tap coefficient fluctuations are unknown, the step size is

generally set to $0 < \mu < 1$. The pole radius with $0 < \sqrt{\rho} < 2$ is set to be slightly less than 1. The notch band, the area removed by the adaptive notch filter narrows as the radius approaches 1 [21].

The distance between a subject's chest and the Doppler radar was set as 1 m, and the subjects were kept in a seated posture. The subjects wore a T-shirt during the experiment. The true heartbeat and respiration rates were measured by a contact-type vital sensor (Equivital Ltd. EQ02) simultaneously with the measurements by the Doppler radar. Each recording is measured for 200 seconds. As the contact-type sensor detects heart rate every 5 seconds, the estimated values are also obtained every 5 seconds for comparison.

A dataset is created for each person for the experiments, comprising eight people as subjects with ages ranging from 21 to 25 years. This experiment on human subjects was approved by the research ethics review committee of the Faculty of Engineering, Tottori University (No. R4-5). Table 2.2 shows each human subject's average value, maximum deviation, and standard deviation of heart rate data, which is detected by the contact-type vital sensor. The maximum deviation is given by

$$Maximun\ Deviation = \max\{\left|HR_{ref}(i) - \overline{HR_{ref}(i)}\right|\},$$

where $\overline{HR_{ref}(i)}$ represents the time-average of $HR_{ref}(i)$. $\max\{\cdot\}$ represents the maximum value of $\{\cdot\}$.

TABLE 2.1: SIMULATION PARAMETERS FOR HUMAN SUBJECTS.

Pole radius ρ_h for $H_h(z)$	0.95
Step size μ_h for $H_h(z)$	0.1
Initial value of estimated heart rate for $\beta_h(0)$	120[bpm]
Pole radius ρ_r for $H_r(z)$	0.99
Initial value of estimated respiration rate for $\beta_r(0)$	20[bpm]
Step size μ_r for $H_r(z)$	0.05

TABLE 2.2: AVERAGE AND DEVIATION OF TRUE HEART RATE FOR HUMAN SUBJECTS.

Subject No	Average	Maximum Deviation	Standard Deviation
1	86.15	3.85	1.98
2	72.17	10.83	2.75
3	77.24	12.76	4.06
4	82.12	6.88	3.19
5	69.32	11.68	5.12
6	85.22	6.78	3.64
7	64.78	38.22	7.71
8	74.88	15.12	4.03

2.4.2 Number of stages and pole radius of RHEF for human subjects

The RHEF $H(z)$ used in the proposed system comprises notch filters connected in a cascade. The number of removed respiration harmonics depends on the number of notch-filter stages. Moreover, the pole radius determines the notch bandwidth. Therefore, the accuracy of heart rate estimation depends on the number of stages and the pole radius of the RHEF $H(z)$.

Fig. 2.3 illustrates the MAPE of heart rate versus the number of stages of RHEF $H(z)$. The MAPE in Fig. 2.3 are obtained by averaging the results of eight subjects. The number of stages in the filter cascade $M = 0$ represents the proposed system without the RHEF. The simulation results show that the error for $M = 2$ is smaller than that for $M = 0$, and the introduction of the RHEF improves the accuracy of heart rate estimation. Unfortunately, the error increases when the number of stages is greater than or equal to three and when the pole radius is reduced. This is because the number of stages is too many and the notch bandwidth is too wide to reduce respiration harmonics; thus, the RHEF distorts a heartbeat component. When $\rho = 0.95$ at the second stage of the cascaded notch filters, the proposed system sufficiently reduces the error. Therefore, $\rho = 0.95$ and $M = 2$ are adopted for the filter cascade.

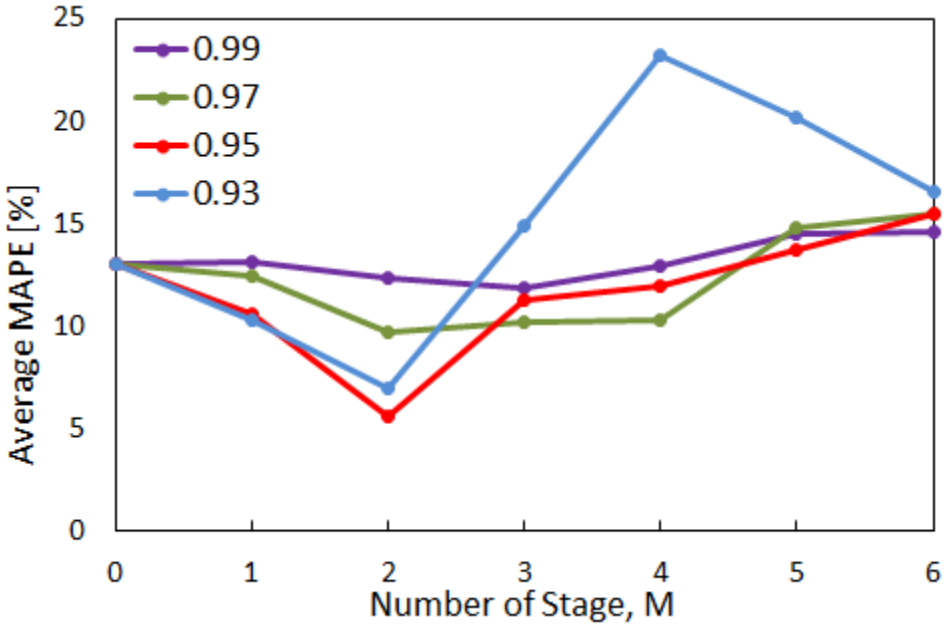

FIGURE 2.3: Average MAPE vs. the number of stages of the RHEF for human subjects.

2.4.3 Experiment results for human subjects

Table 2.3 illustrates the simulation results in heart rate estimation to compare the proposed method with the conventional methods. Each value of the evaluation index is obtained from eight subjects, and the average value represents averaging the results of eight subjects. The proposed method's average MAPE, MAE, MSE, and RMSE are 5.24%, 4.00, 28.38, and 5.26, respectively, and the proposed method obtains the highest accuracy. In addition, all evaluation indexes of the proposed method are lower than any other conventional method in each trial.

Fig. 2.4 shows the estimated heart rate for human subject trial No.1. Fig. 2.4 (a), (b), (c), (d), (e), (f), and (g) illustrate the heart rate estimated using the aforementioned conventional methods. Fig. 2.4 (h) illustrates the estimated heart rate using the proposed system. Fig. 2.5 shows the power spectrums of the input and output signals of the RHEF $H(z)$. Fig. 2.5 (a) and (b) illustrate the power spectrum at 100 and 180 seconds, respectively. Considering Fig. 2.5, the input signal of the RHEF includes a 3rd order respiration harmonic. The frequencies of the 3^{rd} order harmonics are respectively 1.074 Hz (64.44 bpm) at 100 seconds and 1.07 Hz (64.2 bpm) at

180 seconds. Moreover, the contact-type vital sensor indicates heart rates of 1.51 Hz (90.6 bpm) at 100 seconds and 1.46 Hz (87.6 bpm) at 180 seconds.

Fig. 2.4 (a), (b), and (c) show that autocorrelation, FFT, and CWT sometimes can be detect the heart rate accurately; however, they are not always usable. Fig. 2.5 (b) shows that they are not influenced by the 3rd order respiration harmonic, whose power is lower than the heartbeat component. Moreover, the 3rd order respiration harmonic, whose power is higher than the heartbeat component, degrades the estimation accuracy from Fig. 2.5 (a). Fig. 2.4 (d) shows that the time-window-variation method detects the heart rate with a slight error. Fig. 2.4 (e) shows that the spectrogram method degrades estimation performance owing to respiration harmonics and noise. Fig. 2.4 (f) shows that the heart rate estimated by BPFB is off the reference because BPFB traces the 3rd order respiration harmonic in the band of a selected bandpass filter. As indicated by Fig. 2.4 (g), N-DCT cannot reliably capture the true heart rate due to 3rd order respiration harmonics and noise. Fig. 2.4 (h) shows that the proposed method can trace the reference. Fig. 2.5 shows that the RHEF $H(z)$ with cascaded notch filters reduces the 3rd order respiration harmonic, allowing the proposed system to estimate heart rate accurately. In addition, Fig. 2.4 (h) shows that the proposed method using the ANF with an adaptive algorithm is more robust against noise than the time-window-variation method.

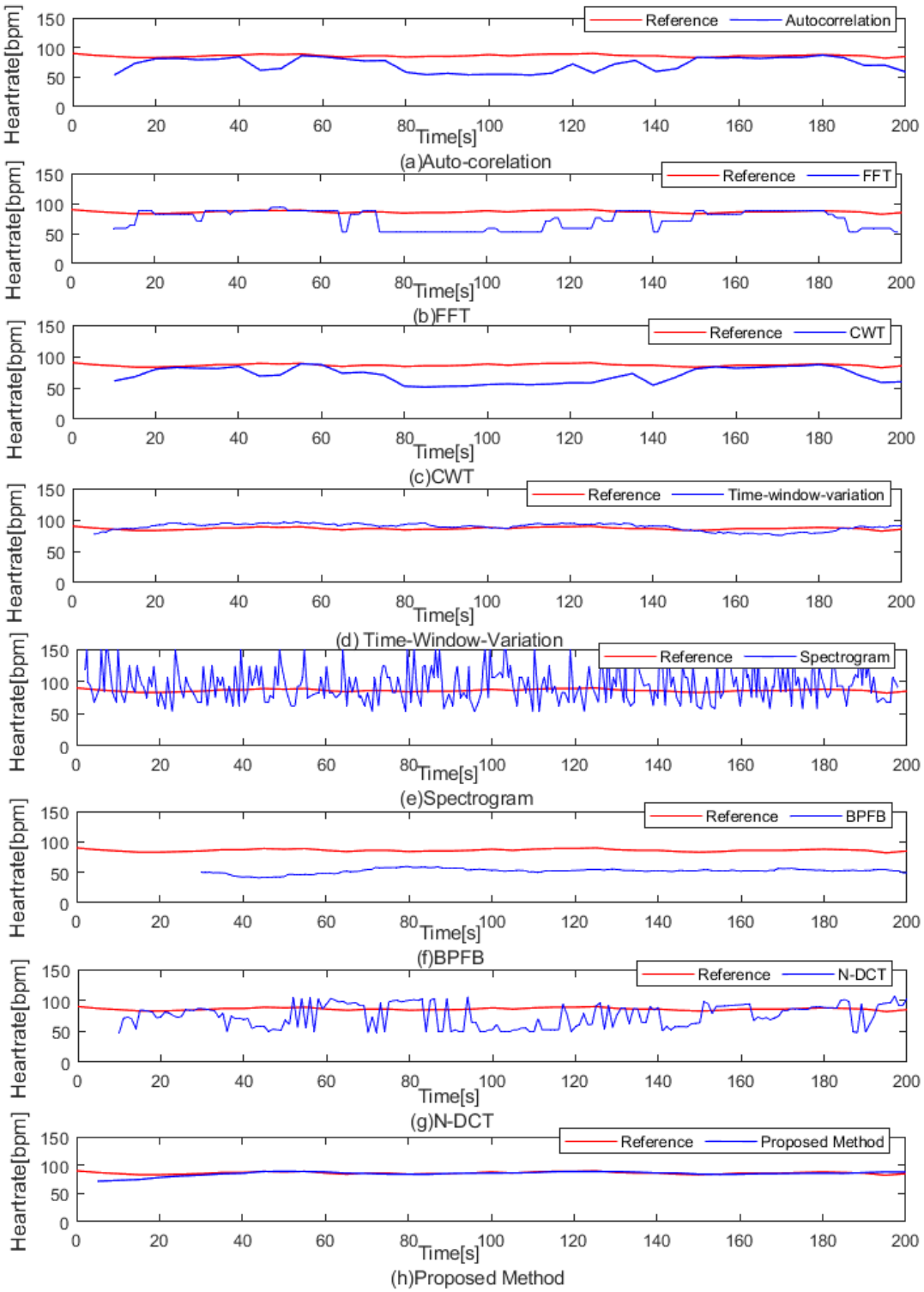

FIGURE 2.4: Estimated heart rate for human subject Trial No 1.

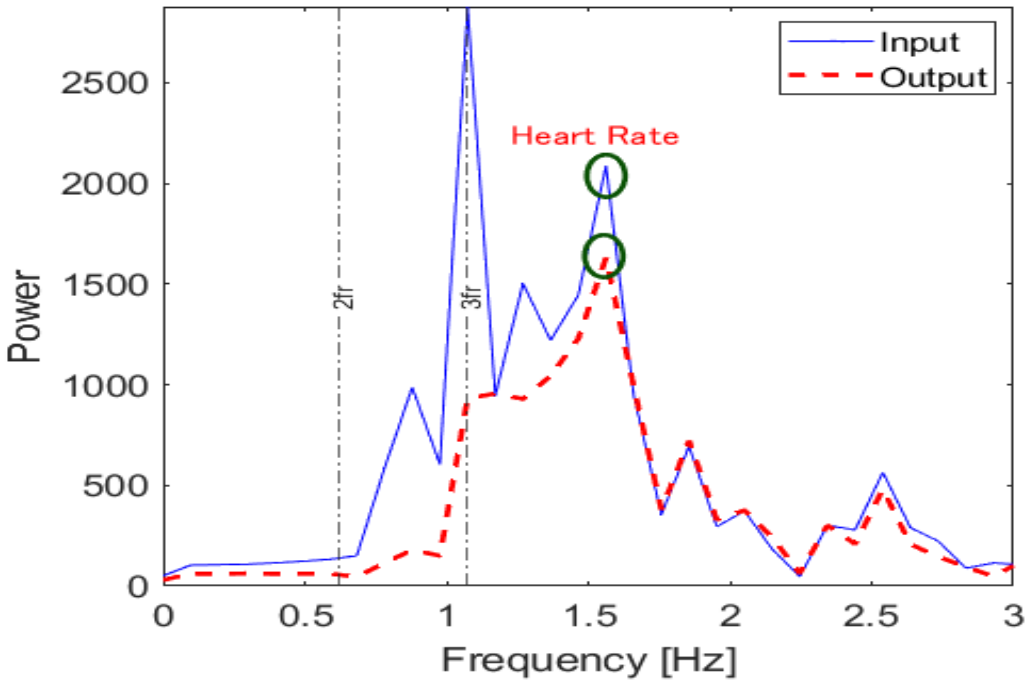

(a) 100 Seconds

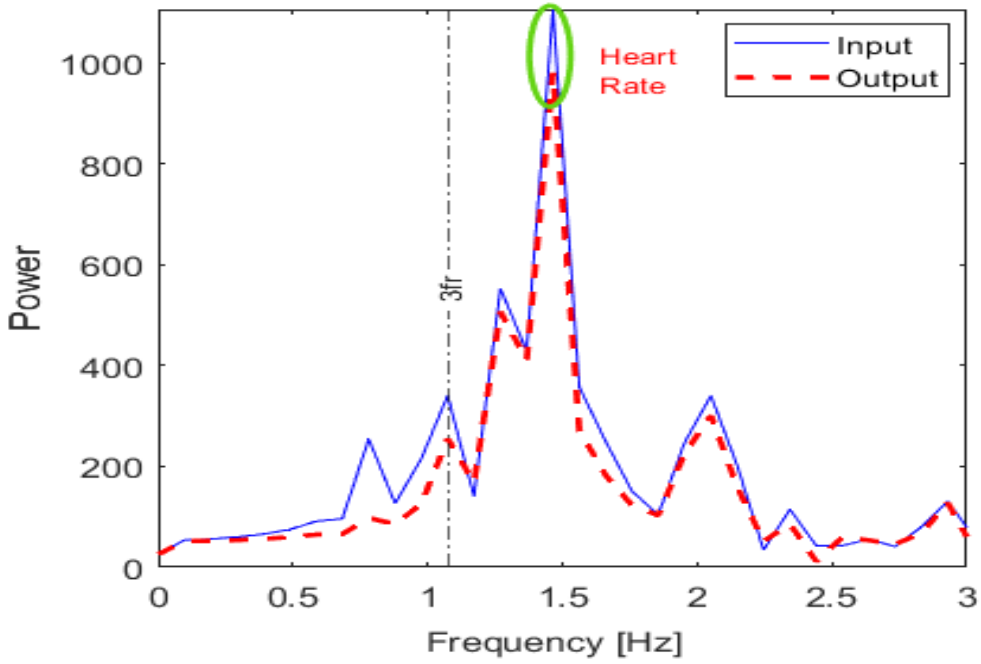

(b) 180 Seconds

FIGURE 2.5: Input and output power spectrums of the RHEF for human subject Trial No. 1.

TABLE 2.3: SIMULATION RESULTS FOR HUMAN SUBJECTS.

Evaluation Index	Subject No	Auto-correlation	FFT	CWT	TWV	Spectrogram	BPFB	N-DCT	Proposed Method
MAPE	**1**	17.13	16.01	18.71	6.56	25.10	39.48	20.30	2.67
	2	8.20	10.40	9.69	24.53	39.58	30.37	23.70	6.32
	3	11.61	18.12	14.67	15.86	27.56	37.32	18.05	5.28
	4	15.30	20.92	17.40	11.69	32.03	38.31	21.14	6.10
	5	8.13	13.18	9.91	29.65	42.62	17.38	23.74	5.36
	6	21.02	26.93	24.71	5.38	22.81	36.80	24.66	4.26
	7	8.25	8.47	8.48	35.70	39.83	21.49	28.72	7.65
	8	12.58	14.07	14.39	19.93	29.00	29.95	19.24	4.29
	Average	12.78	16.01	14.75	18.66	32.32	31.39	22.44	5.24
MAE	**1**	14.81	13.92	16.14	5.64	21.67	34.12	17.53	2.28
	2	5.94	7.51	7.01	17.62	28.57	21.89	17.04	4.52
	3	9.06	13.99	11.44	12.06	21.39	28.69	13.80	4.21
	4	12.73	17.41	14.53	9.51	26.41	31.72	17.40	5.09
	5	5.67	9.38	6.90	20.02	29.32	12.29	16.26	3.63
	6	18.04	23.11	21.09	4.55	19.59	31.54	21.12	3.70
	7	5.72	5.80	5.81	22.55	25.55	14.64	18.69	5.29
	8	9.41	10.55	10.76	14.74	21.43	22.26	14.28	3.28
	Average	10.17	12.71	11.71	13.34	24.24	24.64	17.01	4.00
MSE	**1**	366.14	377.14	412.55	39.79	737.44	1187.30	472.05	14.71
	2	54.27	89.78	73.22	335.23	1552.80	493.24	369.41	34.23
	3	129.41	234.45	181.76	160.25	750.95	834.92	247.97	36.10
	4	221.58	387.35	292.11	115.03	1279.60	1024.70	415.72	37.22
	5	50.62	128.96	64.10	441.55	1400.50	175.57	356.50	18.55
	6	410.01	622.51	520.24	30.69	611.34	1026.10	592.51	26.70
	7	71.10	67.47	62.75	542.85	1156.30	292.92	541.29	37.06
	8	114.82	149.18	148.73	229.65	891.33	539.98	275.95	22.52
	Average	177.24	257.11	219.43	236.88	1047.53	696.84	408.93	28.38
RMSE	**1**	19.13	19.42	20.31	6.31	27.16	34.46	21.73	3.84
	2	7.37	9.48	8.56	18.31	39.41	22.21	19.22	5.85
	3	11.38	15.31	13.48	12.66	27.40	28.90	15.75	6.01
	4	14.89	19.68	17.09	10.73	35.77	32.01	20.39	6.10
	5	7.12	11.36	8.01	21.01	37.42	13.25	18.88	4.31
	6	20.25	24.95	22.81	5.54	24.73	32.03	24.34	5.17
	7	8.43	8.21	7.92	23.30	34.00	17.12	23.27	6.09
	8	10.72	12.21	12.20	15.15	29.86	23.24	16.61	4.75
	Average	12.41	15.08	13.80	14.13	31.97	25.40	20.02	5.26

2.5 Measurement Experiments for Dog Subjects

2.5.1 Measurement Conditions for dog subject

TABLE 2.4: SIMULATION PARAMETERS FOR DOG SUBJECTS.

Pole radius ρ_h for $H_h(z)$	0.95
Step size μ_h for $H_h(z)$	0.1
Initial value of estimated heart rate for $\beta_h(0)$	120[bpm]
Pole radius ρ_r for $H_r(z)$	0.99
Initial value of estimated respiration rate for $\beta_r(0)$	20[bpm]
Step size μ_r for $H_r(z)$	0.05

The performance of the proposed system is evaluated with a beagle dog as a subject. The aim of dog experiments is to evaluate the estimation accuracy of the proposed method under the influence of respiration harmonics and body movement. The dog moves, sits, or lies down in a cage, as well as slightly and rapidly trembles. Table 2.4 lists the parameters of the proposed system used in this experiment.

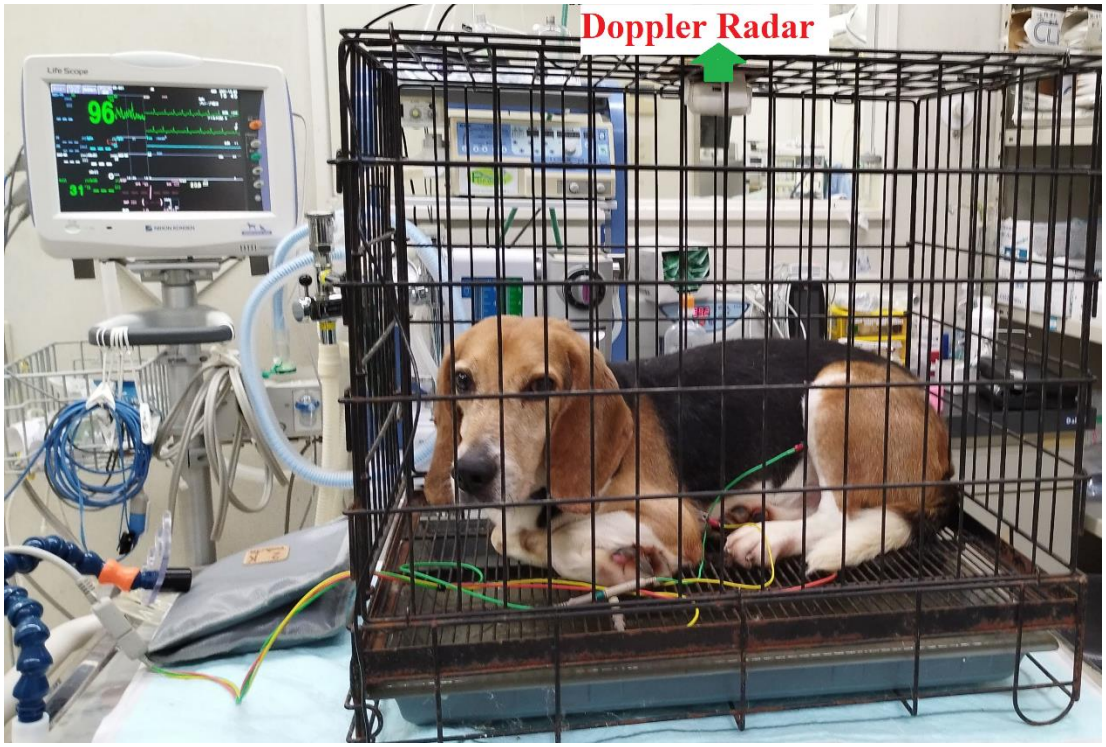

FIGURE 2.6: Scene of data collection for the dog subject.

TABLE 2.5: AVERAGE AND DEVIATION OF TRUE HEART RATE FOR DOG SUBJECTS.

Subject No	Average	Maximum Deviation	Standard Deviation
1	136.93	61.07	14.36
2	161.43	56.57	13.50
3	140.58	58.42	15.60
4	152.07	58.93	16.16
5	135.65	67.35	18.83
6	156.50	63.50	14.24
7	148.96	48.04	13.91
8	136.93	61.07	14.36

A dataset is created that contains seven recordings of a 13-year-old female dog at the Veterinary Medical Center, Tottori University. This experiment on the dog was approved by the Institutional Animal Care and USE Committee, Tottori University (Approval No. 19-T-4). The dog's condition in the experiment differs from that in a daily life environment, and the dog's mood changes from day to day. The Doppler radar is attached vertically downward at the center position of the ceiling of a wire pet cage as shown in Fig. 2.6. The dog is constantly below the radar; however, the distance between the radar and the body surface changes depending on the dog's body posture. When the dog sits, the distance is approximately 5 cm above the head, whereas when the dog lies down, it becomes 30 cm above the abdomen. Each recording is measured for 40 minutes. Simultaneously, the ground truth heart rate is recorded using an electrocardiography-type (ECG) vital sign monitor (Nihon Koden Corp. BSM-3592). Table 2.5 shows each trial's average, maximum, and standard deviation of heart rate data, which are detected by the contact-type vital sensor.

MAPE, MAE, MSE, and RMSE were used for evaluating the estimated heart rate. As the vital sensor detects heart rate every 1 second, an estimated heart rate is set to output every 1 second for comparison. Because a received signal for a dog includes many artifacts due to the misalignment of electrodes, $HR_{ref}(i)$ is obtained using a moving average for 30 seconds to reduce artifacts.

2.5.2 Number of stages and pole radius of the RHEF for dog subject

The effects of respiratory harmonics are different because of the difference in body structures between humans and dogs, and the required number of RHEF stages also differs. Therefore, conduct experiments on the number of RHEF stages for a dog. Fig. 2.7 illustrates the MAPE of heart rate versus the number of stages of the RHEF $H(z)$. The MAPE in Fig. 2.7 are obtained by averaging the results of seven trials. The stage of zero represents the proposed system without the RHEF $H(z)$. The simulation results indicate that the RHEF $H(z)$ effectively improves estimation accuracy. Unfortunately, the error increases when the number of stages is greater than or equal to five for $\rho = 0.93, 0.95, and\ 0.97$. This is because the notch bandwidth is too wide to reduce respiration harmonics; thus, the RHEF distorts heartbeat components.

When $\rho = 0.99$, the proposed system slightly reduces the error because the notch bandwidth is too narrow. Notably, respiration harmonics may remain when the estimated respiration frequency is slightly different from the true respiration frequency. When $\rho = 0.95$ with $M = 4$, the proposed system sufficiently reduces error. Therefore, $\rho = 0.95$ and $M = 4$ are adopted for the RHEF.

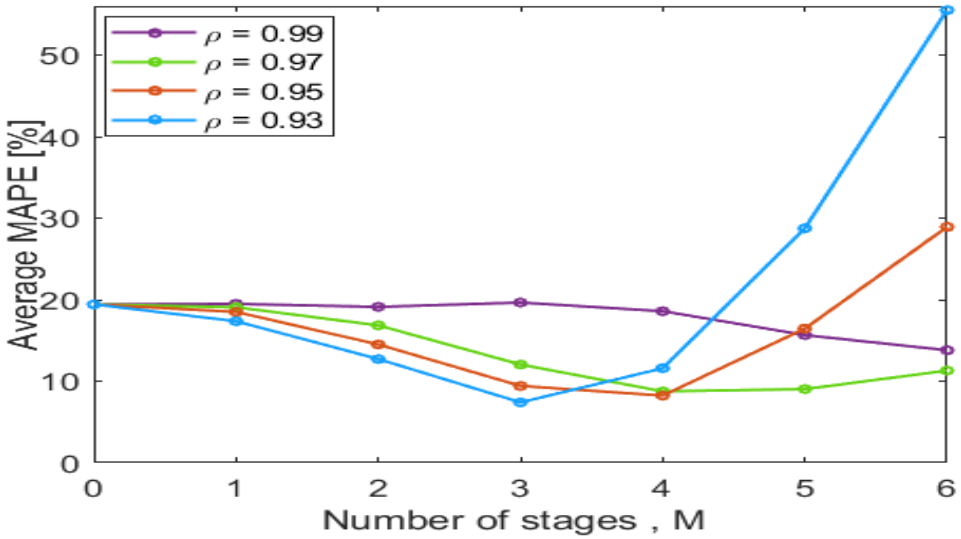

FIGURE 2.7: Average MAPE vs. the number of stages of the RHEF for the dog subject.

2.5.3 Heart rate estimation performance for Dog

The proposed system is compared with conventional systems based on autocorrelation [1], FFT [1], CWT [12], TWV [14], spectrogram method [15], BPFB [16], and N-DCT [18]. The MAPE, MAE, MSE, and RMSE are shown in Table 2.6. The proposed method's MAPE, MAE, MSE, and RMSE are 7.04%, 10.28, 165.31, and 12.58 on average, respectively, and the proposed method obtains higher accuracy than any other method. The proposed method improves the estimation accuracy for all evaluation indexes in each trial.

Fig. 2.8 illustrates the estimated heart rate of trial #7. Fig. 2.8 (a) shows the heart rate obtained from an ECG signal before and after the moving average. Fig. 2.8 (b), (c), (d), (e), (f), (g), and (h) show the heart rate estimated using autocorrelation, FFT, CWT, time-window-variation technique, spectrogram, BPFB, and N-DCT, respectively. Fig. 2.8 (i) illustrates the estimated heart rate using the proposed system. Fig. 2.9 shows the power spectrum of the input and output signals of the RHEF $H(z)$ at 2,230 seconds into trial #7. The RHEF input signal contains components at 1.48 Hz, 1.85 Hz, and 2.3 Hz. As the respiration frequency estimated by the proposed method is 0.37 Hz at 2,230 seconds, the 1.48 Hz and 1.85 Hz components are the fourth and fifth respiratory harmonics. Because the true heart rate measured using the ECG vital sign monitor is 138 bpm (2.3 Hz) at 2,230 seconds, the 2.3 Hz component in Fig. 2.9 is the heart-rate component.

Fig. 2.8 (b), (c), (e), (f), and (h) show that the heart rates estimated with autocorrelation, FFT, time-window-variation, spectrogram, and N-DCT significantly vary because of moving artifacts. Although the heart rates estimated with CWT and BPFB have low dispersion as shown in Fig. 2.8 (d), and (g), respectively, these methods capture the 4th and 5th respiration harmonics. Fig. 2.8 (i) shows that the proposed method tracks true heart rate accurately. As the RHEF $H(z)$ with $M = 4$ reduces the 4th and 5th respiration harmonics as shown in Fig. 2.9, the proposed method improves the estimation accuracy by eliminating respiration harmonics. Moreover, the proposed method is robust against moving artifacts and noise because the heart rates estimated with the proposed method have low dispersion as demonstrated in Fig. 2.8 (i). Simulation results show that the proposed method, which uses ANF and an adaptive algorithm, demonstrably improves the accuracy of heart rate estimation.

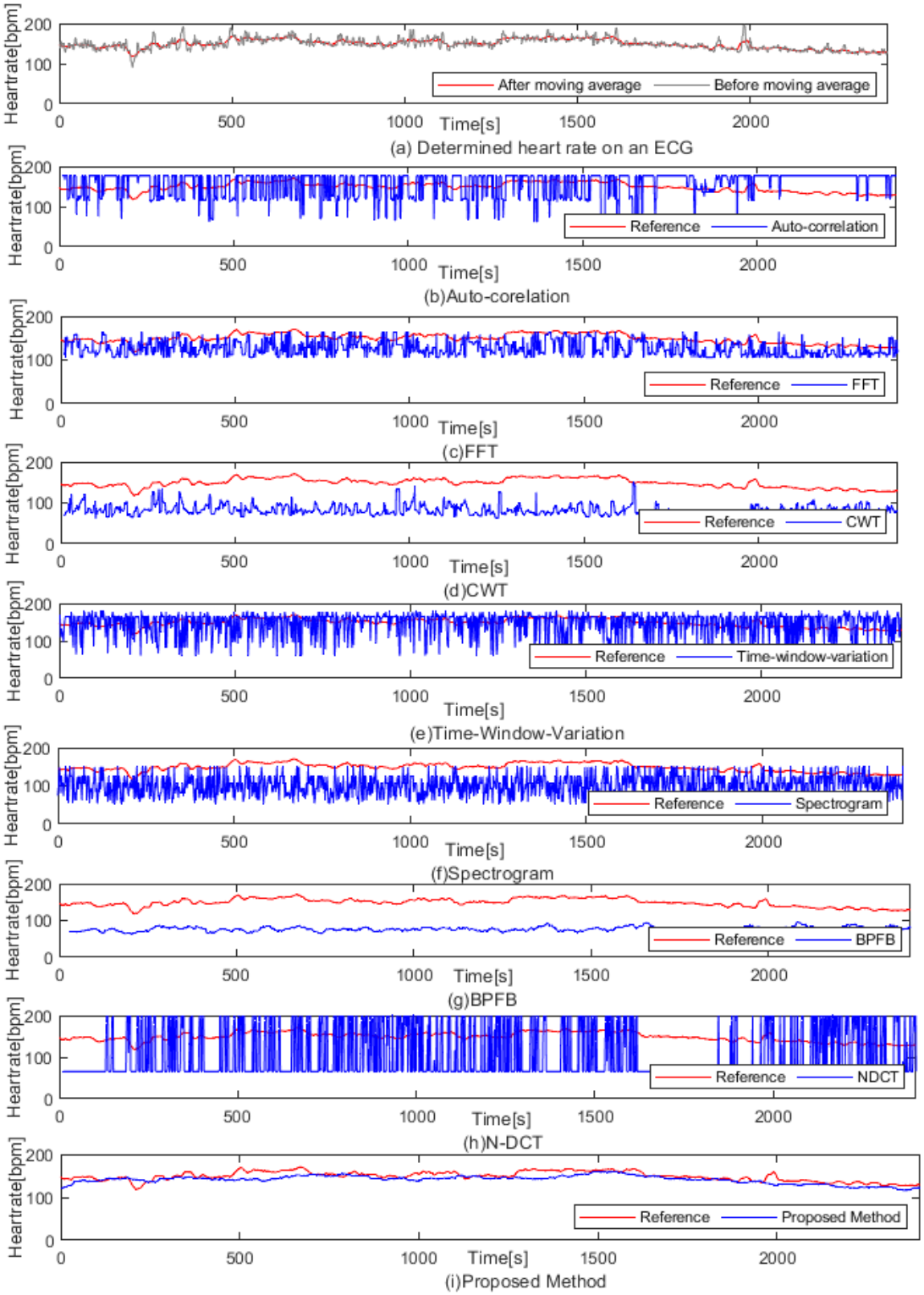

FIGURE 2.8: Estimated heart rate for the dog subject Trial No. 7.

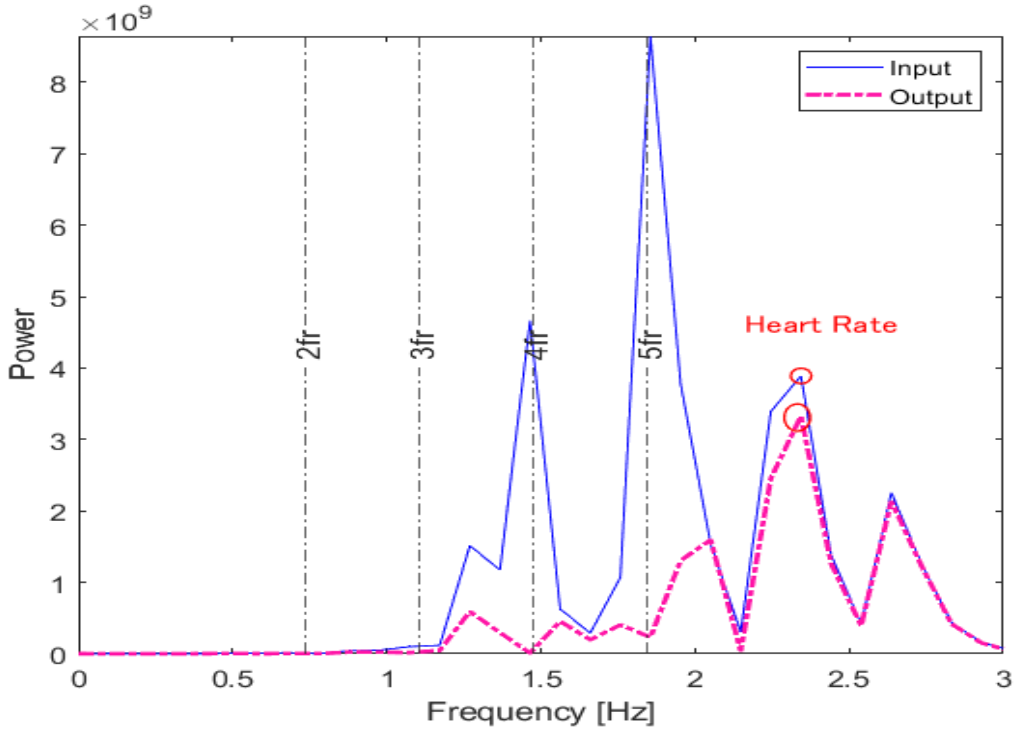

FIGURE 2.9: Input and output power spectrums of the RHEF for the dog subject Trial No. 7 at 2,230 s.

TABLE 2.6: SIMULATION RESULTS FOR DOG SUBJECT.

Evaluation Index	Subject No	Auto-correlation	FFT	CWT	TWV	Spectrogram	BPFB	N-DCT	Proposed Method
MAPE	1	27.08	19.14	39.26	21.54	28.66	43.82	50.27	11.42
	2	16.21	30.77	50.27	15.37	36.45	53.04	48.19	6.10
	3	23.16	18.83	35.63	20.85	29.91	45.14	48.76	6.00
	4	21.16	26.35	45.87	17.66	32.93	49.47	48.20	6.08
	5	26.78	19.89	36.87	23.16	29.91	44.38	49.89	8.43
	6	18.93	28.81	47.46	16.75	35.05	50.96	48.08	5.92
	7	21.74	26.09	44.82	18.53	31.91	48.25	49.17	5.34
	Average	22.15	24.27	42.88	19.13	32.12	47.86	48.94	7.04
MAE	1	36.46	26.53	54.14	29.25	39.67	60.41	68.84	15.17
	2	26.06	49.61	81.37	24.79	59.31	85.96	77.70	10.03
	3	32.34	26.82	50.41	28.98	42.38	63.70	68.57	8.44
	4	31.48	40.22	69.99	26.43	50.99	75.77	73.19	9.36
	5	35.56	27.41	50.34	30.81	41.02	60.81	67.54	11.58
	6	29.45	45.17	74.28	26.02	55.33	80.11	75.27	9.48
	7	31.85	39.07	67.16	27.19	48.13	72.35	73.14	7.89
	Average	31.89	36.40	63.96	27.64	48.12	71.30	72.04	10.28
MSE	1	2E+03	1E+03	3E+03	1E+03	2E+03	4E+03	5E+03	331.06
	2	1E+03	3E+03	7E+03	1E+03	4E+03	8E+03	7E+03	147.96
	3	1E+03	1E+03	3E+03	1E+03	2E+03	4E+03	5E+03	106.56
	4	1E+03	2E+03	5E+03	1E+03	3E+03	6E+03	6E+03	131.47
	5	2E+03	1E+03	3E+03	1E+03	2E+03	4E+03	5E+03	200.57
	6	1E+03	3E+03	6E+03	1E+03	4E+03	7E+03	6E+03	143.41
	7	1E+03	2E+03	5E+03	1E+03	3E+03	5E+03	6E+03	96.11
	Average	1E+03	2E+03	4E+03	1E+03	3E+03	5E+03	6E+03	165.31
RMSE	1	39.04	31.86	56.26	34.99	46.41	61.49	70.65	18.20
	2	32.65	55.84	82.40	36.11	66.42	86.67	82.43	12.16
	3	35.45	32.59	53.95	34.26	49.27	64.48	70.99	10.32
	4	35.73	45.37	71.83	35.33	59.00	77.02	76.87	11.47
	5	39.20	32.56	52.78	35.18	47.87	62.22	69.84	14.16
	6	33.94	50.28	75.59	35.73	62.47	80.80	79.24	11.98
	7	35.62	44.28	69.06	34.96	55.68	73.44	76.00	9.80
	Average	35.95	41.83	65.98	35.22	55.30	72.30	75.15	12.58

2.6 Conclusion

In this chapter, a novel heart rate estimation method is proposed using an ANF and RHEF. Conventional heart rate estimation systems degrade estimation accuracy because of respiration harmonics, moving artifacts, and noise. To this end, the proposed system eliminates respiration harmonics using cascaded notch filters with notch frequencies that are controlled by an estimated fundamental respiration frequency. In addition, an ANF with an adaptive algorithm is adopted to attain robust estimation against moving artifacts and noise. Considering the experimental results for human and dog subjects, the proposed method achieves the best performance in comparison with multiple conventional methods. This indicates that the proposed method demonstrably estimates heart rate accurately without the influence of respiration harmonics, moving artifacts, and noise.

In the future, I will investigate automatically setting hyperparameters and improvement of estimation accuracy for a received signal with intermodulation of respiration and heart rate.

Chapter 3

Non-Contact Heart Rate Measurement Based on Bispectrum Estimation

3.1 Interference Reduction using Bispectrum Estimation

Doppler radar has been acquired as a non-contact heart rate measurement method. There is the possibility to be another person around a subject in an actual environment. The disturbance influence due to another person is treated as a key problem on the estimation of HR. In this chapter, I investigate the suitability of the bispectrum in reducing the influence, to accurately reconstruct the heart-beat signal. The bispectrum is a signal processing technique based on high order statistics. The Bispectrum has two frequency spectra and describes the dependency between these spectra. Thus, I assume that the received signal, which is reflected in a subject, generates a strong phase coupling when the subject is in front of a Doppler radar. On the other hand, the phase coupling of the influence due to an obstructive person is assumed to be weak. Therefore, the bispectrum has the possibility to reduce the influence.

3.2.1 Structure of Heart-Rate-Estimation Based on Two-Dimension Bispectrum

The bispectrum preserves phase information, which is useful for displaying quadratic nonlinear coupling between the different frequency components [35]. Therefore, in cases that the different frequency components are dependent and the phases of the different frequency components are coupled, the bispectrum at the corresponding frequency bin becomes large. In this chapter, a subject is placed in front of a Doppler radar. Therefore, the received signal, which is reflected in a subject, is assumed to generate a strong phase coupling. On the other hand, I assume that the phase coupling of the influence is due to an obstructive person becoming weaker when there is an obstructive person at a different angle from the subject.

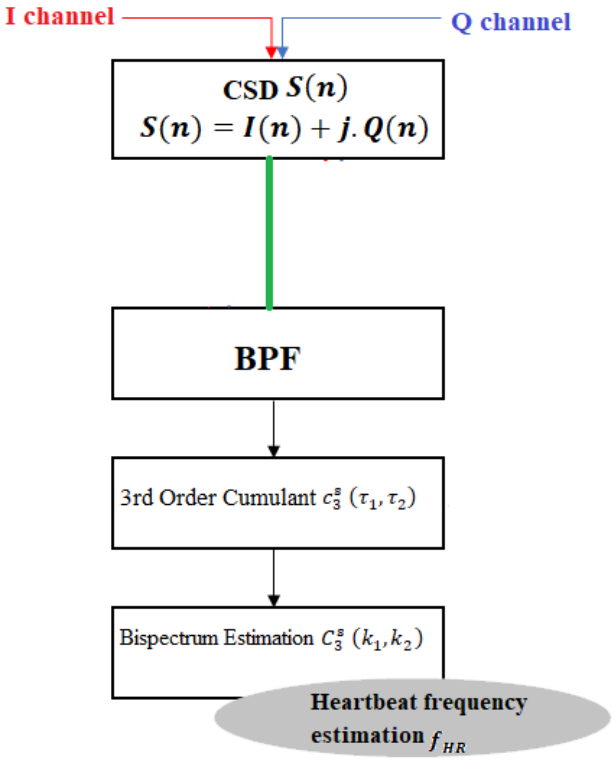

Figure. 3.1 Structure of proposed method

Fig. 3.1 shows the structure of the proposed method. The band pass filter (BPF) is introduced to reduce the disturbance except for the heartbeat component. The BPF limits the pass band from 1.0 Hz to 3.0 Hz.

Next, the third order cumulant of the output signal of BPF, which is given by the following equation, is calculated.

$$c_3^S(\tau_1, \tau_2) =$$

$$m_3^S(\tau_1, \tau_2) - m_1^S[m_2^S(\tau_1) + m_2^S(\tau_2) + m_2^S(\tau_1 - \tau_2)] + 2(m_1^S)^3, \qquad (3.1)$$

where $m_3^x(\tau_1, \tau_2)$ is the third-order moment of $x(n)$. $m_2^x(\tau_2)$ and m_1^x represent the 2nd order moment and 1st order moment. τ_1, τ_2 are delay. These moments are given by

$$m_3^S(\tau_1,\tau_2) = E[S(n)\cdot S(n-\tau_1)\cdot S(n-\tau_2)],$$
$$m_2^S(\tau_1) = E[S(n)\cdot S(n-\tau_1)],$$
$$m_1^S = E[S(n)], \tag{3.2}$$

where $E[\cdot]$ is an expected value.

Bispectrum is given by the Fourier transform of 3rd order moment $c_3^S(\tau_1,\tau_2)$. The bispectrum $C_3^S(k_1,k_2)$ is represented as

$$C_3^S(k_1,k_2) = \sum_{\tau_1=-N/2}^{N/2-1}\sum_{\tau_2=-N/2}^{N/2-1} c_3^S(\tau_1,\tau_2)\cdot exp\{-j(2\pi k_1\tau_1/N + 2\pi k_2\tau_2/N)\}, \tag{3.3}$$

where k_1, k_2 are frequency indexes.

The Bispectrum method uses frequency, which is the bispectrum calculated in the heart rate range has a peak as the estimated value. The bispectrum to be obtained becomes a two-dimensional complex array $N \times N$. It is necessary to decide whether to select the frequency k_1, k_2 peak detected on the plan. Therefore, assuming that the heartbeat component has a strong coupling between the same frequencies, the value of the diagonal component is treated $k_1\ and\ k_2$ is k. The estimated heart rate in the frequency domain is

$$\hat{k} = \underset{k}{argmax}\{C_3(k)\}, \tag{3.4}$$

And the sampling frequency f_s and the desired frequency f_{HR} is expressed by

$$f_{HR} = \frac{f_s}{N}\times \hat{k}\ [Hz], \tag{3.5}$$

The number of beats per minute is obtained by multiplying f_{HR} by 60.

3.2.2 Measurement Experiment

(a) Experiment Conditions

In this experiment, I evaluate estimation accuracy to verify the effectiveness of the proposed method. The Doppler radar device SHARP DC6M4JN3000, whose output frequency is 24 GHz, was used in this experiment. Table 3.1 shows the parameters that are used in this simulation. The number of subjects was 1. An obstructive person was placed in 7 positions, as shown in Fig. 3.2. The place of subject is at a 0° azimuth angle and 2m from a radar device. The place of disturbance is represented (A to G), ones at a time. The disturbance is sitting at 10°, 30°, 60° angle and 0.5m, 1m, 2m distances. At the time of measurement by the doppler radar, the true heart rate was measured by a contact type vital sensor.

TABLE 3.1: PARAMETERS OF THE PROPOSED METHOD

Modulation type	Unmodulated continuous wave
Initial value of heart rate	60[bpm]
Carrier frequency	24 [GHz]
Measured distance	0.5[m], 1[m] and 2 [m]
Measurement time	180 [s]
Number of subjects	1
Sampling frequency	50 [Hz]

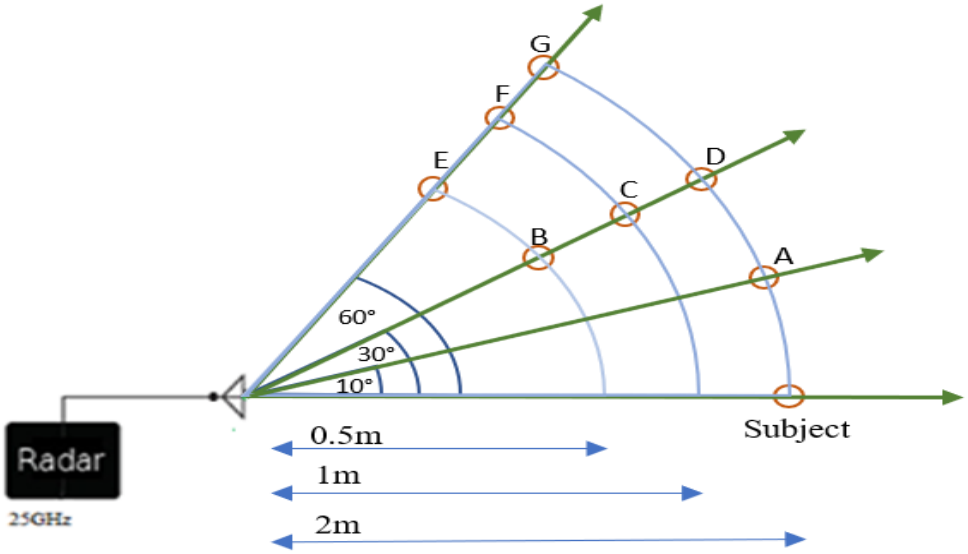

Figure. 3.2 Experimental Setup.

To evaluate the estimated heart rate, use the following root mean square error (RMSE) formula.

$$RMSE = \sqrt{\frac{1}{T}\sum_{t=1}^{T}|HR_r(t) - HR(t)|^2} \ [bpm], \tag{3.6}$$

where $HR_r(t)$ is the estimated heart rate. $HR(t)$ is the heart rate measured by a non-contact type of electrocardiography. T is the number of samples. Since the contact vital sensor detects the heart rate every 5s, the estimated values of the non-contact methods are set as the average value every 5s for comparison.

(b) Experiment Result

In this experiment, I compared the proposed method with the conventional method using a spectrogram [15] and the conventional method using an adaptive notch filter [30]. Fig. 3.3 shows the RMSE. The RMSE obtained by ANF is about 6.0 bpm on average. The conventional method using a spectrogram indicates about 15.2 bpm on average. The RMSE obtained by the proposed method is about 4.2 bpm on average. The proposed method improves the estimation accuracy irrespective of the obstructive person's place.

Fig. 3.4 shows the estimated heart rate. The proposed method and ANF can track the true heart rate. However, the conventional method using a spectrogram comes off as the true value. Fig. 3.5 shows the power spectrum of an output signal of the BPF at 70 seconds. The frequency corresponding to the true heart rate is about 1.0 Hz, which is about 60 bpm. However, the conventional method using a spectrogram has the peak at about 1.4 Hz. Thus, the conventional method using a spectrogram degrades the estimation accuracy. The bispectrum of the output signal of the BPF is shown in Fig. 3.6. The bispectrum has the peak at about 1.0 Hz. From the experimental results, the bispectrum has the potential to reduce the influence component.

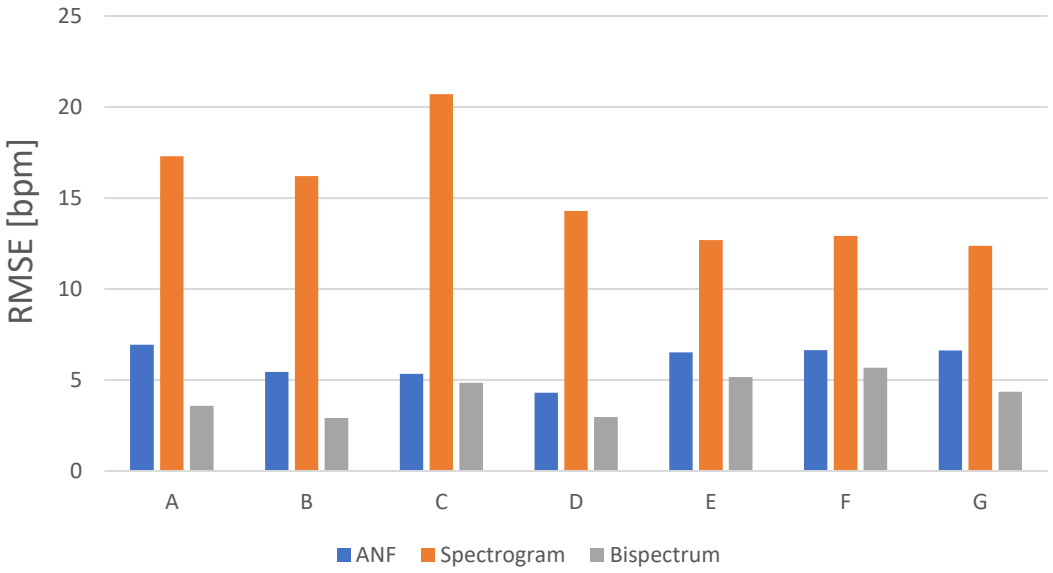

Figure. 3.3 RMSE performance

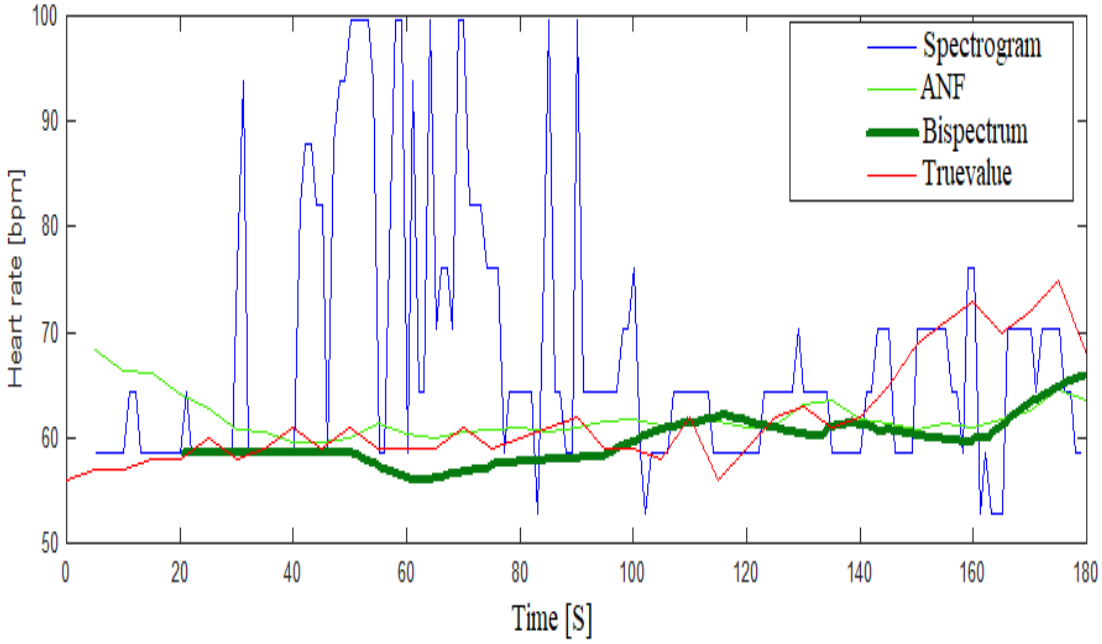

Figure. 3.4 Heart rate measurement by Bi-spectrum and PSD (Position: C).

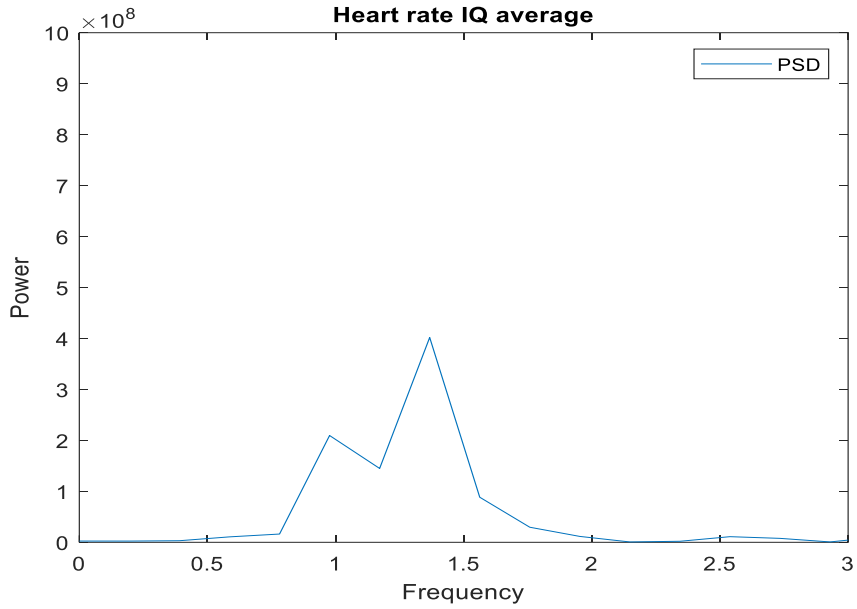

Figure. 3.5 Power Spectrum at 70 sec. (Position: C).

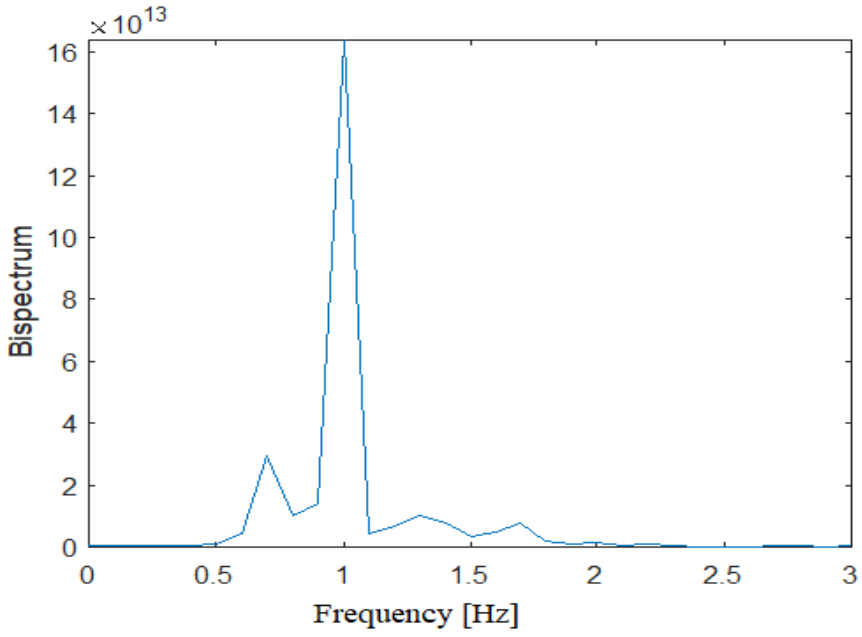

Figure. 3.6 Bispectrum average at 70 sec. (Position: C).

3.2.3 Measurement Experiment for Single Person

TABLE 3.2: PARAMETER OF THE PROPOSED METHOD

Modulation type	Unmodulated continuous wave
Carrier frequency	24 [GHz]
Measured distance	1[m], 1.5[m] and 2 [m]
Measurement time	180 [s]
Number of subjects	1
Sampling frequency	50 [Hz]

(a) Condition

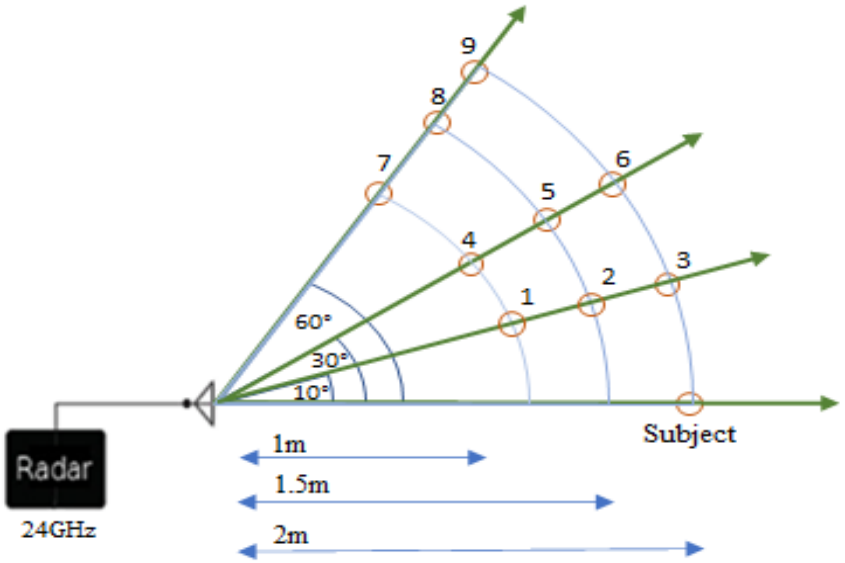

Figure. 3.7 Experimental Setup

I conducted a computer simulation to evaluate the performance of the proposed system for one person. The Doppler radar module used in this experiment was the SHARP DC6M4JN3000, the carrier frequency of which was 24 GHz. Table 3.2 shows the parameters that are used in this simulation. I created a dataset, and the subjects are 5 person whose ages range from 21 to 25 and, the subject wore a T-shirt during the experiment. Fig. 3.7 describes the position of the subject in front of Doppler radar and azimuth angle, also different distances from a radar device. The subject was sitting at 10°, 30°, 60° angle and 1m, 1.5m, 2m distances. Also, I experimented with two persons. One person as a disturbance influence

and sitting with subject ones at a time and sitting position on 10°, 30°, 60° azimuth angle and 1m, 2m distance. The subject and disturbance influence distance was 1m. At that time of measurement, the true heart rate was measured by a contact type equivital sensor. Since the contact type sensor detected the heart rate every 5 seconds, the estimated values were set as the average value every 5 seconds for comparison.

(b) Heart Rate estimation performance of single person

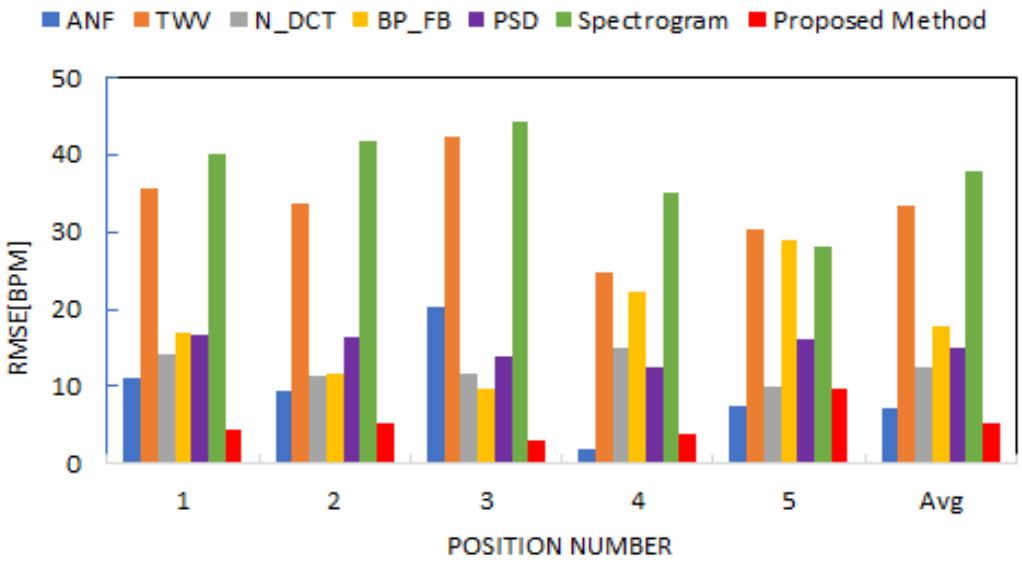

Figure. 3.8 HR-estimation performance of single person front of Doppler Radar

The RMSE results in Fig. 3.8 describe the subject sitting 1m distance from Doppler radar. The average RMSE results for ANF [30], Time-window-variation[14], N_DCT[18], BP_FB[16], PSD[1] and Spectrogram[15] are 7.33%, 33.36%, 12.43%, 17.92%, 15.08% and 37.89% respectively. But our proposed method RMSE is 5.33%.

(c) Heart Rate estimation performance of single persona with and azimuth angle

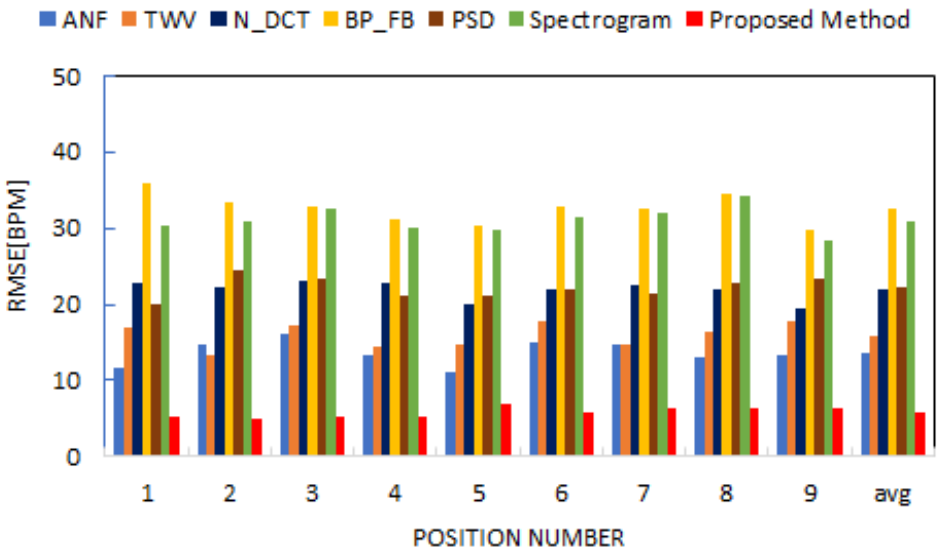

Figure. 3.9 HR-estimation performance of single person with & azimuth angle

The RMSE results in Fig. 3.9 describe the positions 1, 2, 3 are 10° azimuth angle and 1m, 1.5m, 2m distance, 4, 5, 6 are 30° azimuth angle and 1m, 1.5m, 2m distance, 7, 8, 9 are 60° azimuth angle and 1m, 1.5m, 2m distance from Doppler radar. The average RMSE results are 13.70%, 15.94%, 21.87%, 32.62%, 22.17% and 31.02% respectively. And our proposed method RMSE is 5.84%.

(d) Heart Rate estimation performance of two persons, subject with disturbance influence and azimuth angle

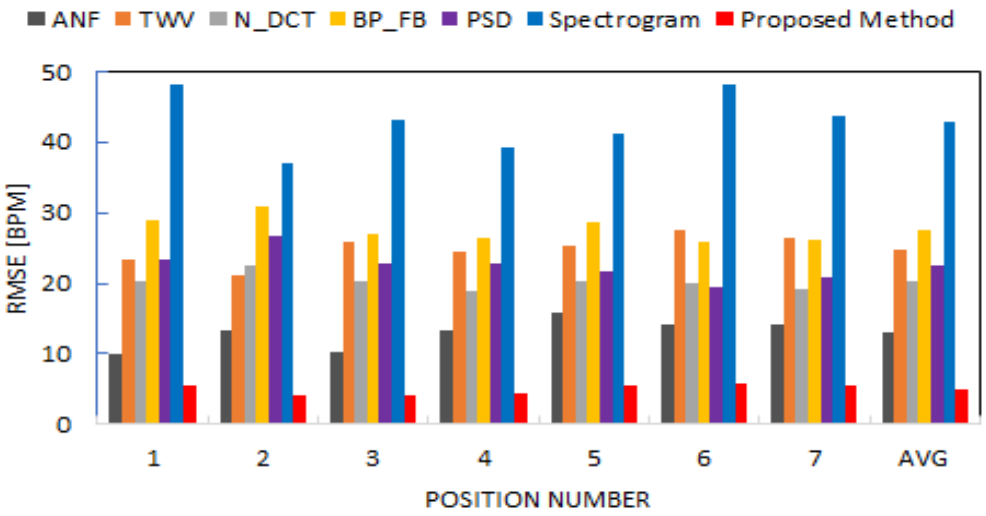

Figure. 3.10 HR-estimation performance of two persons, subject with disturbance influence & azimuth angle

Fig. 3.10 describes the RMSE results of two person's experiments and position 1 is 1m distance from Doppler radar, 2 and 3 are 10° azimuth angles and 1m and 2m distance, 4 and 5 are 30° azimuth angles and 1m, and 2m distance, 6 and 7 are 60° azimuth angles and 1m, and 2m distance from Doppler radar. The average RMSE results are 13.03%, 24.85%, 20.20%, 27.65%, 22.54% and 43% respectively. And our proposed method RMSE is 5.05%.

The heart rate result is shown in Fig. 3.11. In this research, I compared the proposed method with the conventional method. The reference heart rate is 1Hz (60bpm) on average. Fig. 3.11(g) shows the result of bispectrum average heart rate accuracy which is 1Hz. However, the conventional method detected the average heart rate in Fig. 3.11 (a), (b), (c), (d), (e) and (f) are 1.2Hz, 1.8Hz, 0.8Hz, 0.8Hz, 1.6Hz and 2.4Hz respectively. From the experimental results, the bispectrum has the capability to reduce the receiving noise component and detect the heart rate accurately.

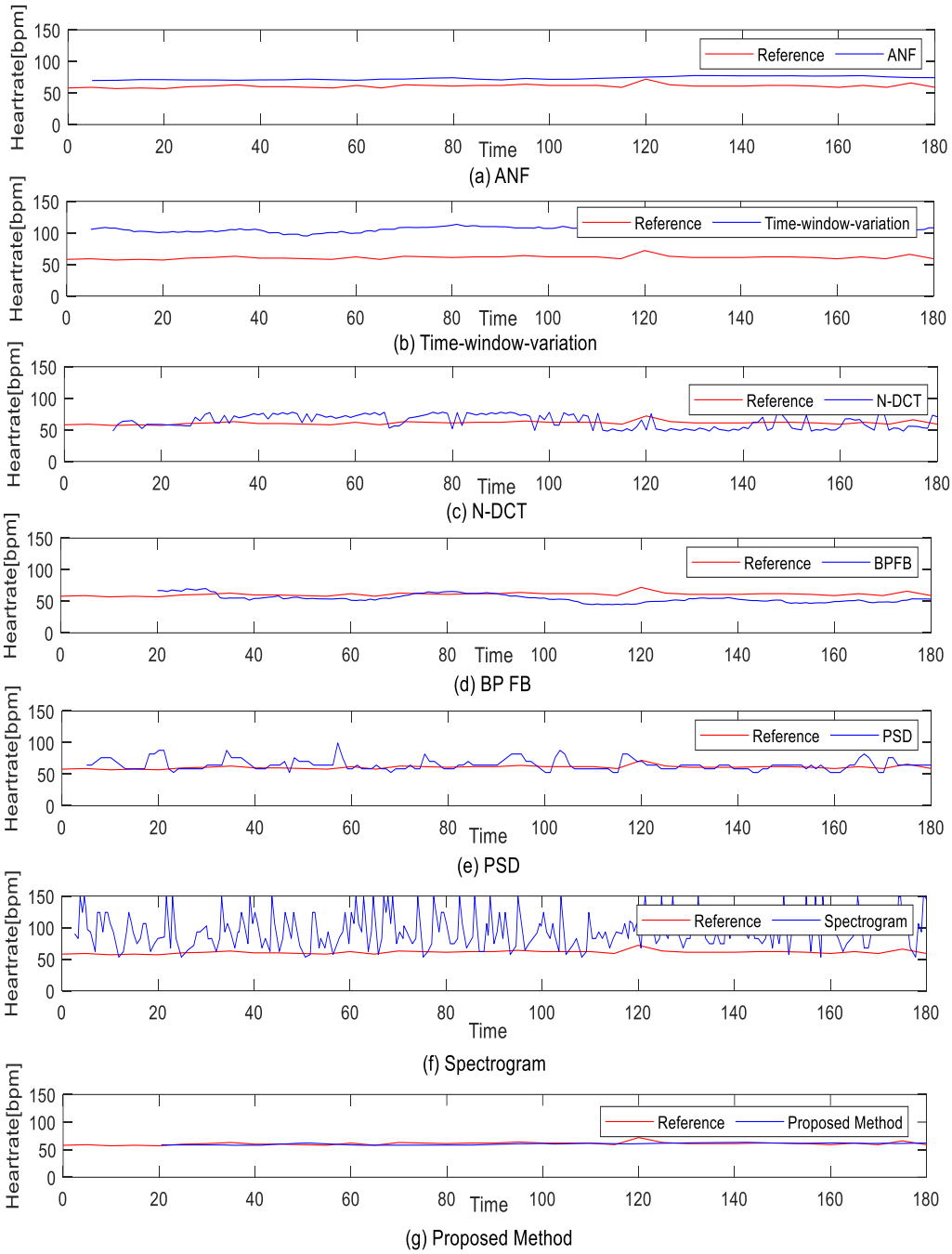

Figure. 3.11 Heart rate Measurement

3.3 Non-Contact Heart Rate Measurement Based on One-dimension Bispectrum Estimation

3.3.1 One-Dimension Estimation

I investigated heart rate measurement based on the bispectrum to reduce the influence of the obstructive person around the subject [37]. Bispectrum has two recurrence spectra and portrays the reliance between these spectra. Therefore, assume that the bispectrum of the component due to an obstructive person is zero. In addition, the bispectrum of white Gaussian noise is zero. Therefore, the bispectrum can detect the heart rate precisely. However, bispectrum increases the computational complexity. Thus, this chapter introduces a one-dimension bispectrum to a heart rate measurement for low computational complexity.

Higher-order cumulants and spectra increase the computational complexity. Therefore, I use one-dimensional slices of multi-dimensional cumulants. One-dimension third-order cumulant is defined by

$$c_3^S(\tau_1,\tau) = m_3^S(\tau_1,\tau) - m_1^S\left[m_2^S(\tau_1) + m_2^S(\tau) + m_2^S(\tau_1-\tau)\right] + 2\left(m_1^S\right)^3, \tag{3.7}$$

where τ is a constant.

From equation (3.7), a one-dimension bispectrum is given by

$$C_3^{S'}(k) = \sum_{\tau=-N/2}^{N/2-1} c_3^S(\tau_1,\tau)\cdot exp^{-j(2\pi k\tau/N)}\ . \tag{3.8}$$

3.3.2Measurement Experiment

(a) Condition

TABLE 3.3: PARAMETER OF THE PROPOSED METHOD

Modulation type	Unmodulated continuous wave
Carrier frequency	24 [GHz]
Measured distance	1 [m]
Measurement time	180 [s]
Number of subjects	1
Sampling frequency	50 [Hz]

I executed a computer simulation to analyze the proposed system's performance. The SHARP DC6M4JN3000 Doppler radar module with a carrier frequency of 24 GHz was used in this experiment. Table 3.3 shows the parameters that were used in this simulation. A dataset was constructed, and the participants were five people aged 21 to 25. Each subject wore a T-shirt during the experiment. The person was seated 1 m away from the Doppler radar device. The research ethics approved this experiment on the human subjects' review committee of the Faculty of Engineering, Tottori University (No. R4-5). A contact-type Equivital sensor was used to measure the true heart rate. The estimated values were set as the average value for every 5 seconds for comparison since the contact type sensor detected the heart rate every 5 seconds.

(b) Measurement Results

Fig. 3.12 shows the RMSE of heart rate measurement results. The average RMSEs for Time-window-variation, Spectrogram, BPFB, and N_DCT are 15.84, 28.96, 24.88, and 20.19 respectively. The average RMSE of a two-dimension bispectrum is 3.73. On the other hand, our proposed one-dimension bispectrum indicates an RMSE of 5.30. Although the performance of the proposed one-dimension bispectrum is slightly lower than the two-dimension bispectrum, it is significantly better than other conventional methods.

The heart rates estimated using Time-window-variation, Spectrogram, BPFB, and N_DCT are shown in Fig. 3.13 (a), (b), (c), and (d). The heart rates estimated by the two-dimension bispectrum and proposed one-dimension bispectrum are shown in Fig. 3.13 (e) and (f). The time-window-variation approach, which utilizes that heart rate does not fluctuate during a short period, detects higher values than the reference values as shown in Fig. 3.13(a). The spectrogram method's estimation performance is degraded by white Gaussian noise, as shown in Fig. 3.13 (b). Since BPFB tracks the noise in the band of a selected band-pass filter, Fig. 3.13 (c) indicates that the heart rate estimated by BPFB is lower than the reference. From Fig. 3.13 (d), N-DCT cannot accurately capture the true heart rate due to respiration noise. The estimated values of the two-dimension and one-dimension bispectrum and reference are respectively 1.18Hz (71bpm) on average. The two-dimension and proposed one-dimension bispectrum can estimate the heart rate accurately as shown in Fig. 3.13 (e) and (f). According to the experimental findings, the one-dimension bispectrum have the ability to decrease the noise component and accurately estimate the heartbeat.

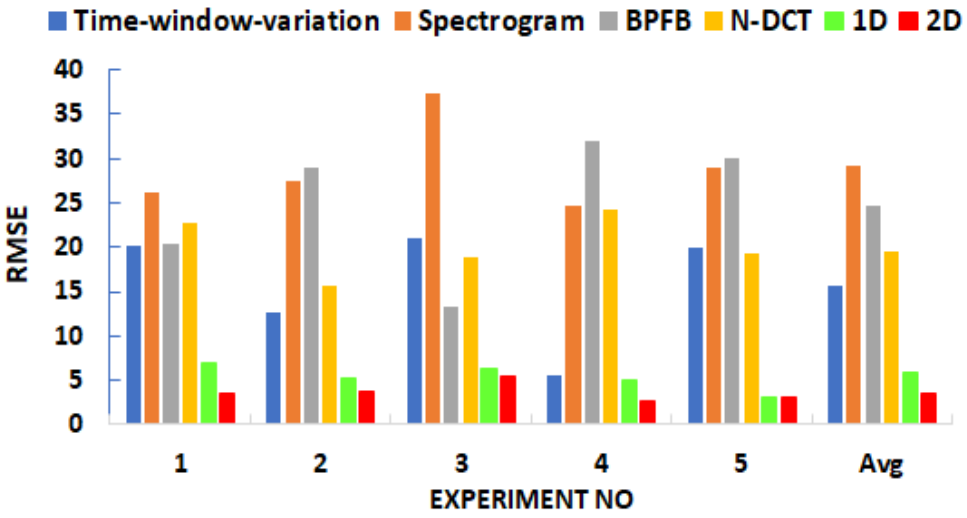

Figure 3.12. Heart rate estimation performance.

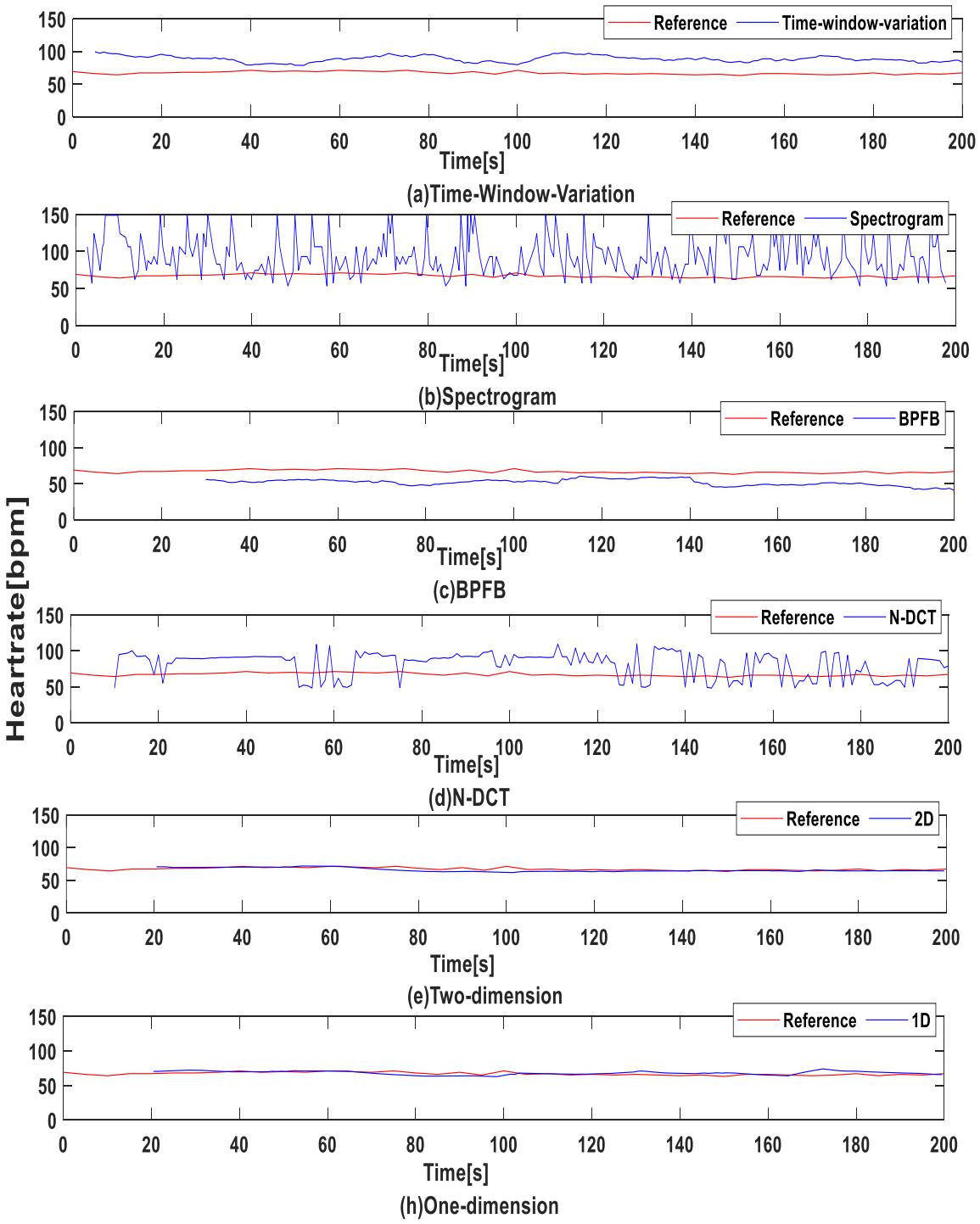

Figure. 3.13 Heart rate Measurement One-dimension

3.4 Conclusion

I investigated the suitability of the bispectrum in reducing the influence and the receiving noise to accurately estimate the heart rate. The bispectrum preserves phase information for describing the quadratic nonlinear coupling between the different frequency components. I observed the suitability of the bispectrum. So, the proposed bispectrum method for detecting heart rate estimation system. Since bispectrum and high-order statistics have zero means for Gaussian noise, hence the bispectrum can improve the performance of the heart rate estimation. However, the bispectrum increases the computational complexity. Thus, here introduced the one-dimension sliced bispectrum. From the simulation results, although the performance of the proposed one-dimension bispectrum is slightly lower than the two-dimension bispectrum. However, One-dimension and two-dimension estimation methods can reduce the noise and detect the heart rate accurately.

In my future work, I will conduct research to improve the performance of the one-dimension and two-dimension bispectrum.

Chapter 4
Conclusion

In recent years, with the onset of an aging society, monitoring biological information has attracted attention. In addition, there is growing interest in monitoring biological information not only in humans but also in animals to detect diseases and changes in physical condition and to check the physical condition after surgery. A common method to obtain biological information is to use contact sensors such as electrocardiograms. However, this contact-type measurement is burdensome because the body of the object to be measured is restrained. Therefore, heartbeat detection using Doppler radar, which can perform non-contact and non-constraint measurements without putting any strain on the body, has been widely studied. This method detects heart rate by observing minute movements of the heart on the body surface. However, heartbeat detection using Doppler radar has the problem that the heartbeat signal is affected by respiratory harmonics and body movement noise, reducing detection accuracy. Therefore, separating the signals caused by the heartbeat from the signals caused by breathing and body movement noise is essential to improving accuracy.

Based on chapter 2, the results of research aimed at improving the accuracy of estimating respiratory rate in subjects and improving the accuracy of estimating heart rate by taking into account the interference of respiratory harmonics.

The results obtained in this research are as follows:

[1] I proposed a method for estimating heart rate and respiration rate and removing respiratory harmonics using an adaptive notch filter for non-contact heart rate and respiration rate detection using Doppler radar. In this method, by using an adaptive notch filter that is effective for estimating narrowband signals, the fundamental frequency due to heartbeat and respiration can be estimated without the limitation of frequency resolution that was a problem with conventional methods. In addition, by using a respiratory harmonic removal filter consisting of cascaded notch filters, it is possible to remove respiratory harmonics that interfere with heartbeat components. The removal notch frequency of the respiratory

harmonic removal filter is determined based on the fundamental frequency of breathing estimated by the adaptive notch filter and is adaptively controlled.

[2] The proposed ANF method was able to reduce the respiration harmonic. The average RMSE results with subjects in a resting state showed that the proposed ANF method was able to improve the heart rate estimation accuracy more than the conventional method.

Based on chapter 3, focused on the difference between the probability distribution of the signal for chest movement. Since it is effective to separate these two signals using skewness, which is a third-order statistic, this is a summary of research conducted with the aim of developing a bispectral heart rate estimation method.

The results obtained in this research are as follows:

[1] The bispectrum in reducing the influence to accurately estimate the heart rate. The bispectrum preserves phase information for describing quadratic nonlinear coupling between the different frequency components. The bispectrum minimizes the interference component that comes from various angles, presuming that the received signal, which is reflected in a subject in front of a Doppler radar, has a significant phase coupling. From the experimental results, the proposed method has the potential to improve the estimation accuracy.

[2] In the bispectrum, it was confirmed that the signal due to heartbeat is distributed in the diagonal component, and the receiving noise is less likely to be distributed in the diagonal component. The bispectrum was observed usefulness for lowering reception noise and precisely estimating heart rate. Therefore, suggest the bispectrum approach for heart rate estimation system detection. Bispectrum and high-order statistics have average values of 0 for white Gaussian noise. Therefore, proposed a heart rate estimation method that is less affected by receiving noise by detecting peaks from the diagonal components of the bispectrum.

[3] This one-dimensional bispectrum-based bispectrum approach measures heart rate without physical contact. Since high-order statistics and bispectrum have zero means for Gaussian noise, bispectrum can enhance the accuracy of heart rate estimates. But the computational complexity is increased by the bispectrum. As a result, the bispectrum was presented in one dimension and sliced.

[4] Experimental results with subjects in a resting state showed that the proposed One-dimension and two-dimension methods were able to reduce the average RMSE of the measured value of the non-contact sensor more than the conventional method, resulting in a heart rate closer to the measured value of the contact sensor. This method was able to improve the accuracy of heart rate estimation, confirming the effectiveness of this method.

Future issues include the development of a method for determining the appropriate number and attenuation amount of respiratory harmonics that interfere with heartbeat components, and a method for removing them. Another challenge is the development of methods to reduce noise.

LIST Of REFERENCES

[1] A. D. Droitcour, "Non-contact measurement of heart and respiration rates with single chip microwave Doppler radar," Ph.D. dissertation to the department of electrical engineering, Stanford University, USA, 2006.

[2] P. -H. Juan, F. -K. Wang, and Y. -T. Tzeng, "SIL-radar-based rat detector for warehouse management system," in Proc. 2019 IEEE MTT-S International Microwave Biomedical Conference, pp. 1--4, 2019, 10.1109/IMBIOC.2019.8777772.

[3] M. Garbey, N. Sun, A. Merla, and I. Pavlidis, "Contact-free measurement of cardiac pulse based on the analysis of thermal imagery," in IEEE Transactions on Biomedical Engineering, vol. 54, no. 8, pp. 1418--1426, Aug. 2007, 10.1109/TBME.2007.891930.

[4] A. Parnandi, and R. Gutierrez-Osuna, "Contactless measurement of heart rate variability from pupillary fluctuations," in Proc. 2013 Humaine Association Conference on Affective Computing and Intelligent Interaction, pp. 191--196, 2013, 10.1109/ACII.2013.38.

[5] W. Verkruysse, L. O Svaasand, and J. S. Nelson, "Remote plethysmographic imaging using ambient light," in Opt. Express, vol. 16, No. 66, pp.21434--21445, 2008.

[6] K. Alghoul, S. Alharthi, H. Al Osman, and A. El Saddik, "Heart rate variability extraction from videos signals: ICA vs. EVM comparison," in IEEE Access, vol. 5, pp. 4711--4719, 2017, 10.1109/ACCESS.2017.2.

[7] S. Sanyal, and K. K. Nundy, "Algorithms for monitoring heart rate and respiratory rate from the video of a user's face," in IEEE Journal of Translational Engineering in Health and Medicine, vol. 6, pp. 1--11, Art no. 2700111, 2018, 10.1109/JTEHM.2018.2818687.

[8] N. Sharma, S. Kaman, and P. K. Mahapatra, "Non-contact measurement of human heart rate using low cost video camera," in Proc. 2019 Fifth International Conference on Image Information Processing, pp. 58--62, 2019, 10.1109/ICIIP47207.2019.8985746.

[9] D. Cho, and B. Lee, "Non-contact robust heart rate estimation using HSV color model and matrix-based IIR filter in the face video imaging," in Proc. 2016 38th Annual International Conference of the IEEE Engineering in Medicine and Biology Society (EMBC), pp. 3847--3850, 2016, 10.1109/EMBC.2016.7591567.

[10] S. Ding, Z. Ke, Z. Yue, C. Song, and L. Lu, "Noncontact multiphysiological signals estimation via visible and infrared facial features fusion," in IEEE Transactions on Instrumentation and Measurement, vol. 71, pp. 1--13, Art no. 40092132022, 2022, 10.1109/TIM.2022.3209750.

[11] C. Li, J. Ling, J. Li, and J. Lin, "Accurate Doppler radar noncontact vital sign detection using the RELAX algorithm," IEEE Trans. Instrumentation and Measurement, vol. 59, no. 3, pp. 687--695, Mar. 2010, 10.1109/TIM.2009.2025986.

[12] A. Tariq, and H. Ghafouri-Shiraz, "Vital signs detection using Doppler radar and continuous wavelet Transform," in Proc. the 5-th European Conference on Antennas and Propagation (EUCAP), pp. 285--288, 2011.

[13] J. Tu, and J. Lin, "Respiration harmonics cancellation for Accurate heart-rate measurement in non-contact vital sign detection," in 2013 IEEE MTT-S International Microwave Symposium Digest (MTT), pp. 1--3, 2013, 10.1109/MWSYM.2013.6697732.

[14] J. Tu, and J. Lin, "Fast acquisition of heart-rate in noncontact vital sign radar measurement using time-window-variation technique," IEEE Trans. Instrumentation and Measurement, vol. 65, no. 1, pp. 112--122, Jan. 2016, 10.1109/TIM.2015.2479103.

[15] E. Mogi, and T. Ohtsuki, "Heartbeat detection with Doppler radar based on spectrogram," in Proc. 2017 IEEE International Conference on Communications (ICC), pp. 1--6, 2017, 10.1109/ICC.2017.7996378.

[16] V. L. Petrović, M. M. Janković, A. V. Lupšić, V. R. Mihajlović, and J. S. Popović-Božović, "High-accuracy real-time monitoring of heart-rate variability using 24 GHz

continuous-wave Doppler radar," IEEE Access, vol. 7, pp. 74721--74733, 2019, 10.1109/ACCESS.2019.2921240.

[17] N. H. Son, H. T. Yen, G. Sun, and K. Ishibashi, "High-accuracy heart rate estimation by half/double BBI moving average and data recovery algorithm of 24GHz CW-Doppler radar," Proc. 2022 International Conference on Advanced Technologies for Communications, pp. 360--363, 2022, 10.1109/ATC55345.2022.9943010.

[18] Z.-K. Yang, H. Shi, S. Zhao, and X.-D. Huang, "Vital sign detection during large-scale and fast body movements based on an adaptive noise cancellation algorithm using a single Doppler radar sensor," Sensors, vol. 20, no. 15, 4183, Jul. 2020, 10.3390/s20154183.

[19] X. Chen, and X. Ni, "Noncontact sleeping heartrate monitoring method using continuous-wave Doppler radar based on the difference quadratic sum demodulation and search algorithm," Sensors, vol.22, no. 19, 7646. 10.3390/s22197646, 2022.

[20] P. A. Regalia, S. K. Mitra, and P. P. Vaidyanathan, "The digital all-pass filter: a versatile signal processing building block," in Proc. the IEEE, vol. 76, no. 1, pp. 19--37, Jan. 1988, 10.1109/5.3286.

[21] P. A. Regalia, "Adaptive IIR Filtering in Signal Processing and Control," NY, USA: Marcel Dekker, 1995.

[22] J. Okello, S. Arita, Y. Itoh, Y. Fukui, and M. Kobayashi, "An adaptive notch filter for eliminating multiple sinusoids with reduced bias," in Proc. 2000 IEEE International Symposium on Circuits and Systems (ISCAS), vol.3, pp. 551--554, 2000, 10.1109/ISCAS.2000.856119.

[23] C. Li, and J. Lin, "Complex signal demodulation and random body movement cancellation techniques for non-contact vital sign detection," in Proc. 2008 IEEE MTT-S International Microwave Symposium Digest, pp. 567--570, 2008, 10.1109/MWSYM.2008.4633229.

[24] Y. Kinugasa, T. Saramäki, Y. Itoh, N. Sasaoka, K. Shiogai, and M. Kobayshi, "Modified subband adaptive notch filters for eliminating multiple sinusoids with reduced bias and faster convergence," in Proc. 2017 IEEE International Symposium on Circuits and Systems (ISCAS), 2017, pp. 1--4, 10.1109/ISCAS.2017.8050871.

[25] S. Haykin, "Adaptive Filter Theory," 3rd., NJ, USA: Prentice Hall, 1996.

[26] T.C. Hsia, and S. Sugimoto, "An investigation of adjustment gain design in stationary and nonstationary LMS adaptive algorithms," IFAC Proceedings Volumes, Vol. 15, No. 4, pp. 1335--1340, 1982, 10.1016/S1474-6670(17)63183-5.

[27] T. Hsia, "Convergence analysis of LMS and NLMS adaptive algorithms," in Proc. IEEE International Conference on Acoustics, Speech, and Signal Processing (ICASSP '83), pp. 667--670, 1983, 10.1109/ICASSP.1983.1172047.

[28] O. Boric-Lubecke, V. M. Lubecke, B. Park, W. Massagram and B. Jokanovic, "Heartbeat interval extraction using doppler radar for health monitoring," 2009 9th International Conference on Telecommunication in Modern Satellite, Cable, and Broadcasting Services, Nis, pp. 139-142, 2009.

[29] M. Nosrati and N. Tavassolian, "High-Accuracy Heart Rate Variability Monitoring Using Doppler Radar Based on Gaussian Pulse Train Modeling and FTPR Algorithm," IEEE Transactions on Microwave Theory and Techniques, vol. 66, no. 1, pp. 556-567, Jan. 2018.

[30] M. Koyama, S. Yamori, N. Sasaoka, Y. Itoh, and D. Takahara, "A Study on Non-contact Heart Rate Measurement with Adaptive Notch Filter and CS, " IEICE technical report, vol. 118, no. 156, BioX2018-13, pp. 33-38, Jul. 2018, (In Japanese).

[31] Changzhi Li and Jenshan Lin, "Complex signal demodulation and random body movement cancellation techniques for non-contact vital sign detection," 2008 IEEE MTT-S International Microwave Symposium Digest, Atlanta, GA, USA, pp. 567-570, 2008.

[32] T. Sakamoto, P. J. Aubry, S. Okumura, H. Taki, T. Sato and A. G. Yarovoy, "Noncontact Measurement of the Instantaneous Heart Rate in a Multi-Person Scenario Using X-Band Array Radar and Adaptive Array Processing," in IEEE Journal on Emerging and Selected Topics in Circuits and Systems, vol. 8, no. 2, pp. 280-293, June 2018.

[33] H. Lee, B. Kim, J. Park, S. W. Kim and J. Yook, "A Resolution Enhancement Technique for Remote Monitoring of the Vital Signs of Multiple Subjects Using a 24 GHz Bandwidth-Limited FMCW Radar," in IEEE Access, vol. 8, pp. 1240-1248, 2020.

[34] W.B. Collis, P.R. White, and J.K. Hammond, "Higher-Order Spectra: The Bispectrum and Trispectrum, " Mechanical Systems and Signal Processing, Vol. 12, No. 3, pp. 375-394, May 1998.

[35] E. Bou Assi, L. Gagliano, S. Rihana, et al. "Bispectrum Features and Multilayer Perceptron Classifier to Enhance Seizure Prediction," Sci Rep 8, 15491, 2018

[36] Z. Yang, H. Shi, S. Zhao &X. Huang, "Vital sign detection during large-scale and fast body movements based on an adaptive noise cancellation algorithm using a single Doppler radar sensor, " Sensor 2020,20,4183

[37] M. Tazen, N. Sasaoka, K. Fujita and Y. Itoh, "Interference reduction using Bispectrum estimation in non-contact heart rate measurement by Doppler radar, " 2020 IEEE Region 10 Conference (TENCON), DOI **:** 10.1109/ TENCON 50793.2020.9293762.

RESEARCH ACHIVEMENT

1. Journal Publication

	Author, Paper Title, Journal, Date	Chapter
1	Moushumi Tazen, Naoto Sasaoka, and Yoshiharu Okamoto, "Non-contact Heart Rate Measurement Based on Adaptive Notch Filter and Elimination of Respiration Harmonics, " IEEE Access, Vol. 11, pp. 46107 – 46119, May.2023, 10.1109/ACCESS.2023.3272895	2

2. Conference Paper

	Author, Paper Title, Conference, Date	Chapter
1	Moushumi Tazen, Naoto Sasaoka, Kasumi Fujita, Yoshio Itoh, "Interference Reduction using Bispectrum Estimation in Non-Contact Heart Rate Measurement by Doppler Radar, " 2020 IEEE region 10 conference (TENCON), pp 964-967, December, 2020	3
2	Moushumi Tazen, Naoto Sasaoka, "Non-Contact Heart Rate Measurement Based on One Dimension Bispectrum Estimation, " 2023 International workshop on Smart Info-Media System in Asia, pp. 144–147, September, 2023	

	IEICE-Tech Report	Chapter
1	Moushumi Tazen, Naoto Sasaoka, Kasumi Fujita, Yoshiharu Okamoto, "Non-Contact Heart Rate Measurement based on Bispectrum, " IEICE-Tech Report, Vol. 121, pp. 68– 71, March.202246107 – 46119, May.2023,	3

CURRICULUM VITAE

Moushumi Tazen graduated in Computer Science and engineering from Northern University, Dhaka, Bangladesh, in 2015. She completed Master`s degree in Information and Electronics, Department of Engineering, Graduate School of Sustainability Science from Tottori University Japan, in 2021. Her research interest is in digital signal processing.